AD-A119 401 ARMY ARMAMENT RESEARCH AND DEVELOPMENT COMMAND ABERD--ETC F/G 21/2
A CONTRIBUTION TO THE FLAT FLAME OLYMPICS: PROBLEM B.(U)
AUG 82 J M HEIMERL
UNCLASSIFIED ARBRL-TR-02416 SBI-AD-F300 073 NL

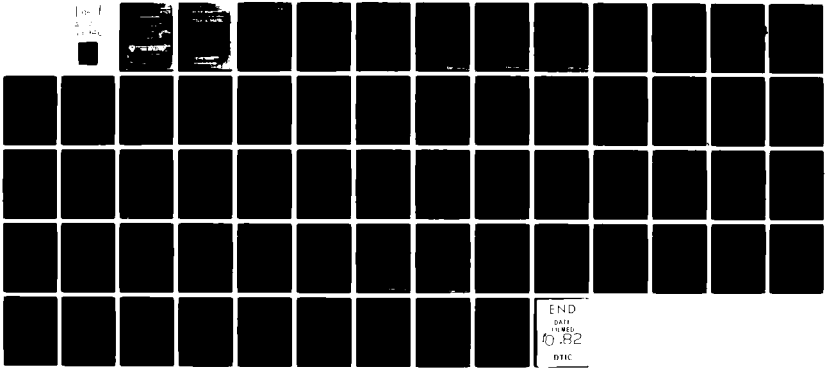

END
DATE FILMED
10-82
DTIC

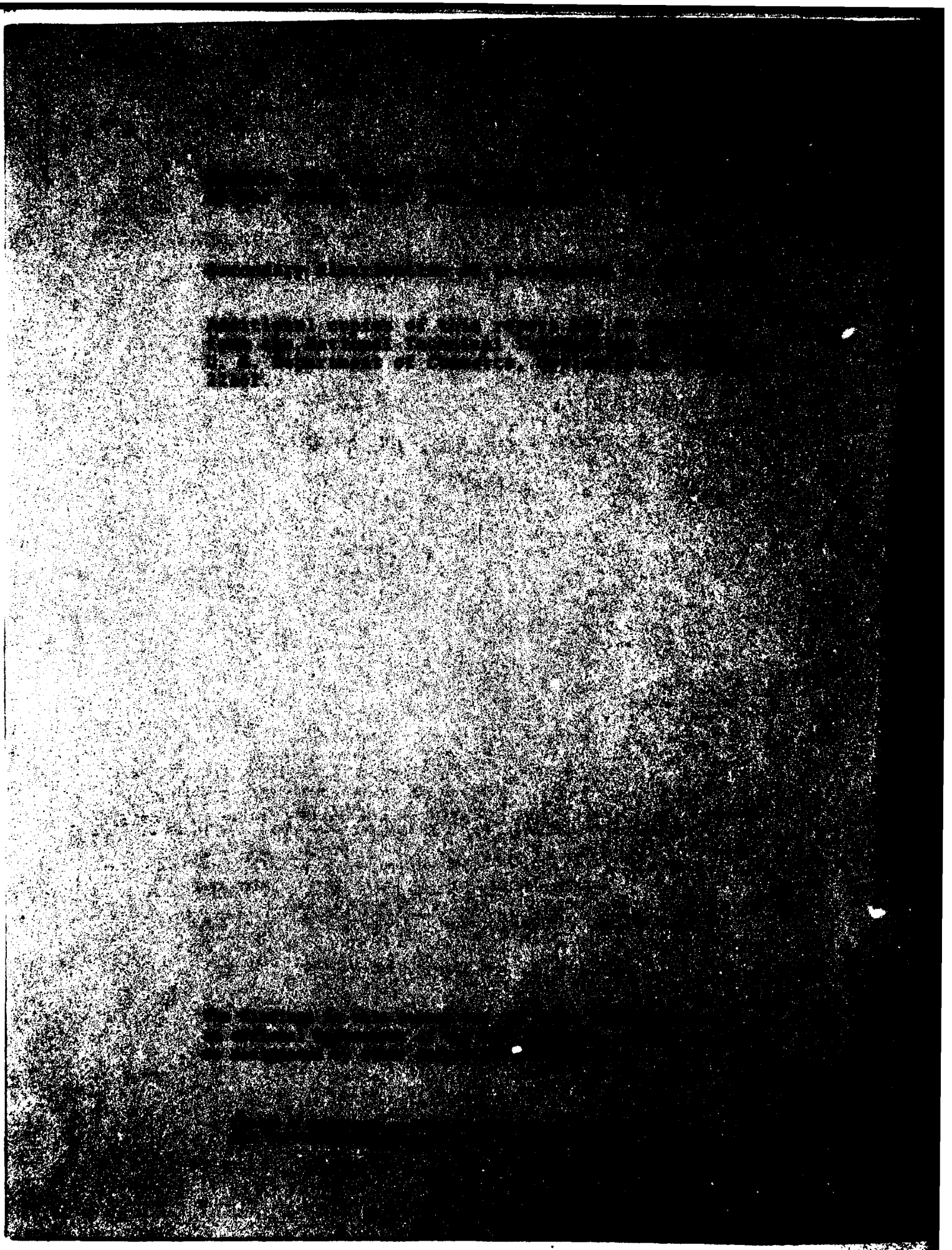

UNCLASSIFIED

SECURITY CLASSIFICATION OF THIS PAGE (When Data Entered)

REPORT DOCUMENTATION PAGE		READ INSTRUCTIONS BEFORE COMPLETING FORM
1. REPORT NUMBER Technical Report ARBRL-TR-02416	2. GOVT ACCESSION NO. AD-A119 401	3. RECIPIENT'S CATALOG NUMBER
4. TITLE (and Subtitle) A CONTRIBUTION TO THE FLAT FLAME OLYMPICS: PROBLEM B.		5. TYPE OF REPORT & PERIOD COVERED Final 6. PERFORMING ORG. REPORT NUMBER
7. AUTHOR(s) Joseph M. Heimerl		8. CONTRACT OR GRANT NUMBER(s)
9. PERFORMING ORGANIZATION NAME AND ADDRESS US Army Ballistic Research Laboratory ATTN: DRDAR-BLI Aberdeen Proving Ground, MD 21005		10. PROGRAM ELEMENT, PROJECT, TASK AREA & WORK UNIT NUMBERS RDT&E 1L161102AH43
11. CONTROLLING OFFICE NAME AND ADDRESS US Army Armament Research & Development Command US Army Ballistic Research Laboratory (DRDAR-BL) Aberdeen Proving Ground, MD 21005		12. REPORT DATE August 1982 13. NUMBER OF PAGES 67
14. MONITORING AGENCY NAME & ADDRESS(if different from Controlling Office)		15. SECURITY CLASS. (of this report) UNCLASSIFIED 15a. DECLASSIFICATION/DOWNGRADING SCHEDULE

16. DISTRIBUTION STATEMENT (of this Report)

Approved for public release; distribution unlimited.

17. DISTRIBUTION STATEMENT (of the abstract entered in Block 20, if different from Report)

18. SUPPLEMENTARY NOTES

Portions of this paper reported at the "GAMM-Workshop on Numerical Methods In Laminar Flame Propagation," University of Aachen 12-14 Oct, 1981.

19. KEY WORDS (Continue on reverse side if necessary and identify by block number)

Premixed Flame	Flame Speed
Hydrogen-Air Flame	Species Profiles
PDECOL	Temperature Profile
Finite Element	Enthalpy Profile

20. ABSTRACT (Continue on reverse side if necessary and identify by block number) (raj)

This report discusses in detail the input parameters used in computing flame speeds and profiles for the stoichiometric hydrogen-air premixed, steady-state, laminar flame. The input kinetics were specified. Our solution was obtained by use of a relaxation technique. The partial differential equations were solved using a finite element method, PDECOL. A special algorithm that enabled spatial grid points to be placed in the flame front was used.

DD FORM 1 JAN 73 1473 EDITION OF 1 NOV 65 IS OBSOLETE UNCLASSIFIED

SECURITY CLASSIFICATION OF THIS PAGE (When Data Entered)

20. Abstract (Cont'd.)

Results include: (1) information requested by the workshop that deals with specific transport parameters, (2) computed flame speeds, (3) mass fraction peak values of radical species profiles, and (4) the extrema of the enthalpy profile. We also consider the likely sources of our computed HO_2 "spike" and OH double peak. We also found features in the N_2 and O_2 mole fraction profiles that are due simply to the mass-to-mole fraction transformation. Finally, we have compared the flame speeds, radical peaks, and enthalpy extrema when two quite different transport mixing algorithms were used. One employs a generalization of Fick's law and $\rho^2 D_{im}$, $\rho\lambda_{mix}$, and c_{pmix} are held constant. The other employs a modified form of the Stefan-Maxwell relations that crudely account for thermal diffusion. Both use the same semi-empirical formulation for λ_{mix}. It is found that the computed results are not sensitive to the transport algorithm used and that most of the differences that are observed can be accounted for by thermal diffusion.

TABLE OF CONTENTS

LIST OF ILLUSTRATIONS

LIST OF TABLES

I. Introduction

A workshop under the direction of Norbert Peters (Instituet fuer Allgemeine Mechanik RWTH Aachen) has been called to focus on numerical methods that have been developed to solve premixed flame problems with complex chemistry and transport properties. The purpose of this workshop is to seek to:

(1) Establish the difficulties that result from non-equal diffusivities of heat and matter and the consequences that these have upon the accuracy of the solution;

(2) Compare different numerical schemes for two test problems; and

(3) Exchange ideas about work in progress. This workshop has been subtitled "The Flat Flame Olympics," and was held 12-14 October, 1981 at the University of Aachen. Proceedings of the entire workshop are to be published.[1a]

This report covers the second test problem: the solution of the steady, stoichiometric hydrogen-air flame with complex chemistry. We have named it the Peters B problem. (The first problem, Peters A, is detailed in another report[1b]). The kinetic scheme and boundary conditions at the cooled end are specified and the governing equations, boundary conditions at the burned end, the initial conditions, transport properties and heat capacities, and numerical scheme were left to the choice of the authors.

This report then documents the choices made and presents material requested for the workshop as well as other interesting findings.

II. The Flame Equations

The derivation of the conservation equations for a multicomponent reacting ideal gas mixture can be found in several texts[1c-3]. Those equations that adequately describe a one-dimensional, laminar, premixed flame that propagates in an unbounded medium are:

Overall continuity

$$\rho_t + (\rho u)_x = 0 ; \tag{1}$$

[1a] *Notes on Numerical Fluid Mechanics, Vol. 5, N. Peters and J. Warnatz, Ed., Vieweg-Verlag, Pub.*

[1b] *T.P. Coffee, "Flat Flame Olympics: Test Problem A," BRL Report to be published.*

[1c] *Hirschfelder, J.O., Curtiss, C.F., and Bird, R.B., Molecular Theory of Gases and Liquids, 2nd Ed. (corrected with notes), Wiley, New York, 1964.*

[2] *Bird, R.B., Stewart, W.S. and Lightfoot, E.N., Transport Phenomena, Wiley, New York, 1960.*

[3] *Williams, F.A., Combustion Theory, Addison-Wesley, Reading, MA, 1965.*

Continuity of species

$$\rho(Y_k)_t + \rho u (Y_k)_x = (\rho Y_k V_k)_x + R_k M_k \qquad k = 1,2,\ldots, N: \tag{2}$$

and conservation of energy,

$$\rho c_p T_t + \rho u c_p T_x = (\lambda T_x)_x - \sum_{k=1}^{N} h_k R_k M_k + \sum_{k=1}^{N} h_k (\rho Y_k V_k)_x \tag{3}$$

where the variables are defined in the glossary. The effects of radiation, viscosity, thermal diffusion and body forces have been neglected and since the burning velocity is small compared to the local speed of sound, the pressure is taken to be constant[3-4]. Our general thrust is the determination of species and temperature profiles and of burning velocities. The boundary conditions are the following (t>o). For $x = -\infty$; $T = T_u$ and $Y_k = Y_{ku}$, k=1,2,..., N, and for $x = +\infty$

$$T_x = (Y_k)_x = 0 \quad (k = 1,2, \ldots). \tag{4}$$

In order to avoid solving Eq (1), a coordinate ψ is introduced such that

$$\psi(x,t) = \int_o^x \rho(x',t)dx'. \tag{5}$$

Then $\psi_x = \rho$ and $\psi_t = -\rho u + m_o(t)$,

where $(\rho u)|_{x=o} = m_o(t)$. With this coordinate change equations (2) and (3) become

$$(Y_k)_t + m_o(Y_k)_\psi = (\rho Y_k V_k)_\psi + R_k M_k / \rho \tag{6}$$

and

$$(T)_t + m_o(T)_\psi = c_p^{-1}\{(\rho\lambda T_\psi)_\psi - \sum_{k=1}^{N} R_k M_k h_k / \rho\}, \tag{7}$$

respectively. In practice convenient dimensionless forms of equations (6) and (7) are solved.

The burning velocity, S_u, is defined as the velocity of the flame relative to the fluid at rest, that is, at "infinity." The value of S_u can be found from the steady-state profiles by performing a coordinate transformation such that the flame appears stationary. In this new system all variables are independent of time, specifically, $(Y_k)_t = \rho_t = 0$. Then from Equation (1) we have $(\rho u)_x = 0$ or ρu = constant. Take any one of the equations (2) and integrate over the interval (a,b) to obtain:

$$\rho u [Y_k(b) - Y_k(a)] = \int_a^b R_k M_k dx - \rho Y_k V_k|_a^b, \tag{8}$$

Then

$$u(-\infty) = \frac{\int_a^b R_k M_k dx - \rho Y_k V_k|_a^b}{\rho(-\infty)[Y_k(b) - Y_k(a)]} = \frac{\int_a^b \rho^{-1} R_k M_k d\psi - \rho Y_k V_k|_a^b}{\rho(-\infty)[Y_k(b) - Y_k(a)]}. \tag{9}$$

[4] *Fristrom, R.M. and Westenberg, A.A., Combustion Theory, Addison-Wesley, Reading, MA, 1965.*

In this coordinate system $S_u = -u(-\infty)$.
One could also take Eq. (3) and integrate it over (a,b) to find an expression similar to Eqs. (8) and (9). Specifically, we have

$$u(-\infty) = - \frac{\int_a^b \sum_{k=1}^{N} R_k M_k h_k dx + \lambda T_x \Big|_a^b}{\rho(-\infty) \int_a^b c_p dT} \tag{10}$$

which for constant c_p reduces to

$$u(-\infty) = - \frac{\int_a^b \sum_{k=1}^{N} R_k M_k h_k dx + \lambda T_x \Big|_a^b}{\rho(-\infty)\, c_p [T_b - T_a]} \quad . \tag{11}$$

For the transport method used below $h_k = c_{pk} T_x = c_p T_x$ and the sum $\sum_{k=1}^{N} h_k (\rho Y_k V_k)_x$ in Eq. (3) vanishes, since $\sum_{k=1}^{N} Y_k V_k = 0$.

The boundary conditions of the unburnt mixture have been specified as: T = 298.15K for a stoichiometric hydrogen-air mixture. Since the overall chemical equation can be written

$$2H_2 + O_2 + N_2 = 2H_2O + N_2$$

and since air is composed[5] of 79% N_2 and 21% O_2, we find the mole (mass) fractions at the unburnt boundary to be: $X_{O_2} = 0.1479$ (0.2264), $X_{H_2} = 0.2958$ (0.0283) and $X_{N_2} = 0.5563$ (0.7453).

The boundary conditions of the burnt mixture are

$$T_x = (Y_k)_x = 0 \quad (k = 1,2,\ldots), \tag{12}$$

The Adiabatic flame temp, T_B, is 2383°K as computed by the NASA-Lewis Code[6].

To define the starting profiles we let ψ_L and ψ_R be the left and right boundaries of the integral of integration. Then define[7]

$$\psi_1 = \psi_L + 0.24\ (\psi_R - \psi_L). \tag{13a}$$

$$\psi_2 = \psi_L + 0.64\ (\psi_R - \psi_L). \tag{13b}$$

---

[5] *The composition of dry air is by mole %: 78.084 N_2, 20.946 O_2, 0.934 Ar, 0.033 CO_2, 0.003 rare gases. See Matheson Gas Data Book, 5th Ed. by W. Braker and A.L. Mossman, Matheson Gas Products, E. Rutherford, N.J. 1971, p. 9.*

[6] *Gordon, S. and McBride, B.J., Computer Program for Calculation of Complex Chemical Equilibrium Compositions, Rocket Performance, Incident and Reflected Shocks and Chapman-Jouquet Detonations, NASA-SP-273, 1971, (1976 program version).*

[7] *Coffee, T.P. and Heimerl, J.M., BRL Technical Report ARBRL-TR-02212, Jan. 1980.*

and

$$Y_K(\psi) = \begin{cases} Y_{ku}, & \psi_L \le \psi \le \psi_1 \\ Y_{ku} + (Y_{kB} - Y_{ku}) \sin\left(\frac{\pi}{2}\left(\frac{\psi - \psi_1}{\psi_2 - \psi_1}\right)^2\right)^2, & \psi_1 \le \psi \le \psi_2 \\ Y_{kB}, & \psi_2 \le \psi \le \psi_R. \end{cases} \tag{13c}$$

T is defined similarly. The choice of the particular function that defines the Y_k and T between ψ_1 and ψ_2 is not important. We have used a straight line with success, but defining a smooth function is slightly more efficient.

III. The Numerical Solution

A modification of the PDECOL package was used to solve this problem[8]. PDECOL, a rather general package for solving one-dimensional differential equations, employs the method of lines in finding a solution.

Spatial discretization is accomplished by finite element collocation methods based on B-splines. The basic assumption is that the solution can be written in the form

$$Y_k \tilde{=} \sum_{i=1}^{NC} C_k(i)\,(t)\, B_i(\psi), \quad k = 1,\ldots,N \tag{14a}$$

and

$$T \tilde{=} \sum_{i=1}^{NC} C_{N+1}(i)\,(t)\, B_i(\psi), \tag{14b}$$

where the basis functions $B_i(\psi)$, i=1,...,NC are B-splines and span the solution space for any fixed t to within a small error tolerance. The time-dependent coefficients $C_k(i)$ are determined uniquely by requiring that the preceding expansion satisfy Eqs. (6) and (7) exactly at (NC -2) interior (collocation) points. The boundary conditions, Eq. (4), are also converted into ordinary differential equations. If there is a null boundary condition, an extra collocation point is added. The B_i are piecewise polynomials of order KORD. The user supplies a set of NB breakpoints (i.e. a set of strictly increasing locations where the polynomials are joined) and the value for NCC, the number of continuity conditions to be applied at the breakpoints. From this information PDECOL generates a set: NC = KORD(NB-1) - NCC(NB-2) basis functions and collocation points. Since by definition a B-spline is zero except over a small interval, at any collocation point no more than KORD of the B-splines are nonzero. So the system of ODE's for the coefficients $C_k(i)$ is not fully coupled.

This system is integrated in time by using a variant of the Gear integrator. It is at this point in the solution that we have modified the PDECOL package[8]. Normally all the Y_k's and T would be solved simultaneously. This procedure would consume inordinate amounts of computer storage. Since we are interested

[8] *Coffee, T.P., BRL Memorandum Report to be published.*

only in steady-state solutions, we have adapted the method of successive calculation. At each time step this process considers each PDE in turn and values for other dependent variables are taken from the most recent computation. In the steady-state this procedure is justified because $(Y_k)_t = T_t = 0$ and the system is in fact decoupled in time.

The code requires the selection of the following parameters. The thermal, ψ-space and temporal normalization factors were taken to be 1000K, 5×10^{-5} gm cm^{-2} and 1×10^{-3} sec, respectively. ψ_0, the cold boundary location is taken to be zero while ψ_5 the normalized "boundary at infinity" is taken to be 2.90.

The time integration is controlled by a user supplied error tolerance ε. Single step error estimates divided by $CMAX_k(i)$ will be kept less than ε in the root-mean-square norm. In the present case ε was chosen as 3×10^{-5}. In PDECOL, $CMAX_k(i)$ is initially set to the maximum of $|c_k(i)|$ and 1.0. Thereafter, $CMAX_k(i)$ is the largest value of $|c_k(i)|$ seen so far, or the initial $CMAX_k(i)$ if that is larger. This error criterion is not appropriate for flames.

In a flame, radical species with relatively small concentrations will control the flame, and we want to compute these accurately. However, some species concentrations at some locations will approach zero, and we do not want to waste time computing a negligible concentration very accurately.

So we will use a semi-relative error control. $CMAX_k(i)$ will be chosen as the maximum of $c_k(i)$ and a user supplied parameter SREC. So concentrations less than SREC will be computed less accurately. Here we have used SREC = 10^{-6}.

The major difficulty in efficiently solving the flame equations is choosing an appropriate set of breakpoints. These must be close enough that spatial errors do not destroy the solution yet not so dense that one's computer resources are exceeded. The breakpoints should be densest in the flame front, where the gradients are very steep.

This problem can be dealt with by working with m_0, the mass flux through the origin. This can be iteratively modified to match the mass flux through the flame. It can also be modified to move the flame front towards the center of the interval of integration, if necessary. The details of this procedure are discussed in Reference 7.

So we may choose our breakpoints to be densest in the center of our interval of integration, we have developed a procedure to generate this type of breakpoint sequence.

The user must supply NINT, the number of intervals (NB = NINT - 1), NCN, the number of intervals of equal length that will be the center of the interval, and FC, the ratio between the longest intervals (on the boundaries) and the shortest intervals. Also let L be the total length of the interval of integration.

The program generates a set of intervals whose lengths increase by a constant factor α, where

$$\alpha = \log^{-1} (2(\log FC)/(NINT - NCN)). \qquad (15a)$$

The common length LC of the NCN center shortest intervals is

$$LC = L/(NCN + 2\alpha\ (\alpha^{(NINT-NCN)/2}-1)/(\alpha-1)). \qquad (15b)$$

Some experimentation is necessary to choose the proper values of the above parameters. In the present case we have chosen NINT = 24, NCN = 6 and FC = 6. Finally the order of the B-splines KORD is taken to be 4 and the number of continuity conditions at the collocation points, NCC, is set equal to 2.

The code was executed on the BRL CYBER 76 system: it required approximately 122000_8 words small core memory and took about 100 seconds to run from a restart file.

IV. Input Coefficients

Kinetics

The steady-state, stoichiometric, plane hydrogen-air flame defined by Peters has the kinetic parameters given in Table 1. ($k = BT^n \exp(C/T)$ in units of cm, mol, s, K.) As a check on the operation of the code we employed another kinetic network listed by Dixon-Lewis[9]. These parameters are given in Table 2. We remind the reader that, at this time, Table 2 contains our best understanding of the $H_2/O_2/N_2$ system and that Table 1 is a simplified set for the purposes of this exercise.

Thermodynamics

The enthalpy and heat capacity are functions of species and of temperature. The JANAF values for the eight species H, OH, O, HO_2, H_2, O_2, H_2O and N_2 are adequately described by the polynomial fits of Gordon and McBride[6]. These fits take the form

$$H_T^o = R\ (a_o + \sum_{n=1}^{5} a_n T^n/n) \qquad (16a)$$

and

$$C_p = R \sum_{n=1}^{5} a_n T^{n-1} \qquad (16b)$$

where the coefficients are listed in Table 3 The heat capacity and specific heat at 2000K are listed in Table 4 and were requested for use at the workshop.

When the values from these polynomials are compared to the tabular values[10-12], those for HO_2 agree to better than 3.6% while all the others agree to better than 1%.

[9] *Dixon-Lewis, G., Philos. Trans. Roy. Soc. (London) 292, 45-99, 1979.*

[10] *JANAF Thermochemical Tables, 2nd Ed. by D.R. Stull and H. Prophet, NSRDS-NB37, June 1971.*

[11] *Chase, M.W., Curnutt, J.L., Hu , A.J., Prophet, H., Syverud, A.N., and Walker, L.C., J. Chem. Ref. Data 3, 311-480, 1974.*

[12] *Chase, M.W., Curnutt, J.L., Prophet, H., McDonald, R.A., and Syverud, A.N., J. Phys. Chem. Ref. Data, 4, 1-175,1975.*

Table 1. Peters' H_2-Air Kinetics

#	Reaction	B	n	C	Ref.
1	$H_2 + OH = H_2O + H$	2.2(13)	0	-2590	A,p77
2	$O_2 + H = O + OH$	2.2(14)	0	-8450	A,p9
3	$H_2 + O = H + OH$	1.8(10)	1.0	-4480	A,p49
4	$OH+OH = H_2O + O$	6.3(12)	0	-550	A,p119
5.	$H+H+M = H_2+M$	6.4(17)	-1	0	A,p299*
6.	$OH + O+M = HO_2+M$	5.(16)***	0	0	A,p411
7.	$O_2+H + M = HO_2 + M$	1.5(15)	0	+550	A,p377**
8.	$HO_2+H = OH + OH$	2.5(14)	0	-950	A,p145
9.	$HO_2 + H = H_2+O_2$	2.5(13)	0	-350	A,p161
10.	$OH + HO_2 = H_2O+O_2$	1.5(13)****	0	0	A,p251
11.	$HO_2 + O = O_2 + OH$	6.3 (13)	0	-350	B,p173

* Values listed are for argon as third body.
** Values listed are for helium or argon as third body.
*** Value of Petersen & Kretschmer at 300°K; for M = O_2
**** Appears estimated based on Leeds values.

A - Evaluated Kinetic Data For High Temperature Reactions by D.L. Baulch, D.D. Drysdale, D.G. Horne, A.C.L. Lloyd, Vol. I, CRC Press, Cleveland, 1972.

B - Evaluated Kinetic Data for High Temperature Reactions, by D.L. Baulch, D.D. Drysdale, J. Duxbury and S.J. Grant, Vol. 3, Butterworth, Boston, 1976.

Table 2. The $H_2/O_2/N_2$ Kinetic Scheme of Dixon-Lewis

#	Reaction	B	n	C
1	$OH + H_2 = H_2O+H$	1.17(9)	1.3	-1825
2	$H + O_2 = OH+O$	1.42(14)	0.0	-8250
3	$O + H_2 = OH+H$	1.8 (10)	1.0	-4480
4	$H+O_2+H_2 = HO_2+H_2$ [c]	1.03(18)	-0.72	0.0
5	$H+HO_2 = OH+OH$	1.4(14)	0.0	- 540
6	$H+HO_2 = O+H_2O$	1.0(13)	0.0	- 540
7	$H+HO_2 = H_2+O_2$	1.25(13)	0.0	0.0
8	$OH+HO_2 = H_2O+O_2$	7.5(12)	0.0	0.0
9	$O+HO_2 = OH+O_2$ [a]	1.4(13)	0.0	- 540
10	$O+HO_2 = OH+O_2$ [a]	1.25(12)	0.0	0.0
11	$H+H+H_2 = H_2+H_2$	9.2(16)	-0.6	0.0
12	$H+H+N_2 = H_2+N_2$	1.0(18)	-1.0	0.0
13	$H+H+O_2 = H_2+O_2$	1.0(18)	-1.0	0.0
14	$H+H+H_2O = H_2+H_2O$	6.0(19)	-1.25	0.0
15	$H+OH+M = H_2O+M$ [b]	1.6(22)	-2.0	0.0
16	$H+O+M = OH+M$ [b]	6.2(16)	-0.6	0.0
17	$OH+OH = O + H_2O$	5.75(12)	0.0	- 390

[a] Dixon-Lewis defines the rate coefficient for $O + HO_2 = OH + O_2$ as $k_9 + k_{10}$.

[b] Value for $M=H_2, N_2$ or O_2; XS for $M=H_2O$.

[c] Chaperon efficiencies relative to H_2 = 1.0 are 0.44, 0.35 and 6.5 for N_2, O_2 and H_2O, respectively.

TABLE 3. THERMODYNAMIC COEFFICIENTS.

SPECIES	RANGE	A0	A1	A2	A3	A4	A5
H	U	.25474390E+05	.24999996E+01	.70881143E-09	-.38728927E-12	.85096613E-16	-.65768080E-20
	L	.25474390E+05	.25000002E+01	-.19925608E-08	.54929899E-11	-.64292197E-14	.26794037E-17
OH	U	.39647060E+04	.29131230E+01	.95418248E-03	-.19084325E-06	.12730795E-10	.24803941E-15
	L	.36715807E+04	.38365518E+01	-.10702014E-02	.94849757E-06	.20843575E-09	-.23384265E-12
O	U	.29230265E+05	.25352638E+01	-.14371898E-04	-.11360139E-07	.66005131E-11	-.61181626E-15
	L	.29143654E+05	.29558662E+01	-.17061536E-02	.25925154E-05	-.17837980E-08	.45709012E-12
HO2	U	.11888500E+04	.37866280E+01	.27885404E-02	-.10168708E-05	.17183946E-09	-.11021852E-13
	L	.13803331E+04	.35094850E+01	.11499670E-02	.58784259E-05	-.77795519E-06	.29607883E-11
H2	U	-.87738042E+03	.31001901E+01	.51119464E-03	.52644210E-07	-.34909973E-10	.36945345E-14
	L	-.98890474E+03	.30574451E+01	.26765200E-02	-.58099162E-05	.55210391E-08	-.18122739E-11
O2	U	-.12019825E+04	.36219535E+01	.73618264E-03	-.19652228E-06	.36201558E-10	-.28945627E-14
	L	-.10475226E+04	.36255985E+01	-.18782184E-02	.70554544E-05	-.67635137E-08	.21555993E-11
H2O	U	-.29905826E+05	.27167633E+01	.29451374E-02	-.80224374E-06	.10226682E-09	-.48472145E-14
	L	-.30279722E+05	.40701275E+01	-.11084499E-02	.41521160E-05	-.29637404E-08	.80702103E-12
N2	U	-.90586184E+03	.28963194E+01	.15154866E-02	-.57235277E-06	.99807393E-10	-.65223555E-14
	L	-.10611588E+04	.36748261E+01	-.12081500E-02	.23240102E-05	-.63217559E-09	-.22577253E-12

U=1000-6000K
L= 300-1000K

Table 4. Heat Capacity and Specific Heat at 2000K.

Species	C_p(cal/mole-K)	c_p(Joule/gm-K)
H	4.968	20.79
OH	8.275	1.923
O	4.976	1.301
HO_2	12.906	1.636
H_2	8.173	17.10
O_2	9.045	1.183
H_2O	12.199	2.8356
N_2	8.609	1.286

TRANSPORT

Individual Species

There are two classes of transport parameters; λ_i, the heat capacity of the ith species, and D_{ij}, the binary diffusion coefficient. We consider them in turn.[13]

The theoretical expression describing the thermal conductivity of hard sphere (i.e., atomic species) is simply related to the viscosity; specifically,

$$\lambda_i M_i/\eta_i = 15R/4. \tag{17}$$

To account for the fact that energy storage in a polyatomic molecule can take place through modes other than translational we have examined the Eucken and modified Eucken correlations. In general form,

$$\lambda_i M_i/\eta_i = f_{tr} C_{tr} + f_{int} C_{int,i} \tag{18}$$

where f_{tr} is set equal to 5/2 so that this expression reduces to the monatomic case (i.e. when $f_{int} = 0$, there $C_{tr} = 3/2R$). $C_{int,i}$ is taken to be $C_{v,i}-C_{tr}$ and there remains the evaluation of f_{int}. Eucken set f_{int} to unity. Others have suggested that the flow of internal energy is a type of diffusional transport and have found that $f_{int} = (Sc)^{-1}$, where the Schmidt number, Sc, is $\eta/\rho D_s$. D_s the self diffusion coefficient, $= 1.20\ \rho\eta\Omega^{(2,2)}/\Omega^{(1,1)}$ (here the ideal gas has been assumed). Since the ratio of collision integrals is approximately 1.1 and is almost independent of temperature, we find $(Sc)^{-1} = 1.32$. This value ($f_{int} = 1.32$) leads us to the modified Eucken correlation.

Usually experimental values of λ_i for non-polar gases lie between the values calculated by the two Eucken forms and so we have elected to take the arithmetic mean of the two forms.

The ensuing expression reduces to

$$\lambda_i = \frac{\eta_i}{M_i} \quad \frac{1.20R + 2.32\ C_{pi}}{2} \quad , \tag{19}$$

where we have used the relation $R = C_p - C_v$. C_p can be computed from the thermodynamic coefficients of Gordon and McBride[6], Eq. 16b.

We see from Eq. 19 that to find the expression for λ_i, we need to find the expression for η_i.

The viscosity of the ith species is given by:

$$\eta_i(\text{gm-cm}^{-1}\text{S}^{-1}) = 2.699 \times 10^{-5}\ (M_i T)^{\frac{1}{2}}/\sigma_i^2 \Omega^{(2,2)}(T_i^*) \tag{20}$$

---

[13] *The discussion follows that of Reid, R.C. and Sherwood, T.K., The Properties of Gases and Liquids, 2nd Ed. McGraw-Hill, N.Y., 1966. Viscosity Chap. 9, Thermal Conductivity, Chap. 10 and Diffusion Coefficients, Chap. 11.*

where $T_i^* \equiv (\varepsilon/k)_i^{-1} T$. The Lennard-Jones (or Stockmayer, in the case of H_2O) parameters are given in Table 5.

TABLE 5. LENNARD-JONES/STOCKMAYER PARAMETERS

Species	σ (10^{-8}cm)	ε/k (°K)	Remarks
H	2.05	145	a
OH	2.947	127.2	like O
O	2.947	127.2	b
HO_2	3.372	128.7	like O_2
H_2	2.92	38.0	a
O_2	3.372	128.7	b
H_2O	2.60	572	a
N_2	3.62	97.5	a

[a] J. Warnatz "Calculation of the Structure of Laminar Flat Flames II: Flame Velocity and Structure of Freely Propagating Hydrogen-Oxygen and Hydrogen Air-Flames" Ber. Bunsengs Phys. Chem. 82, 643-649 (1978).

[b] J.M. Heimerl and T.P. Coffee, "The Detailed Modeling of Premixed Laminar Steady-State Flames. I Ozone." Combustion and Flame 39, 301-315 (1980).

In order to evaluate the collision integrals for polar molecules not only is ε/k required but also the dimensionless parameter

$$\delta = \mu_{H_2O}^2 \Big/ \left(2\, \varepsilon_{H_2O}\, \sigma_{H_2O}^3 \right). \tag{21}$$

The dipole moment for H_2O, μ_{H_2O}, is taken to be 1.844 Debye (1 Debye $\equiv 10^{18}$ dyne$^{\frac{1}{2}}$-cm^2). This value agrees with those reported by McCellan[14] (1.82) and Nelson[15] et al. (1.85). With this value for μ_{H_2O} and the parameters from Table 4 we find $\delta = 1.225$.

---

[14] *McCellan, A.L., Tables of Experimental Dipole Moments, Freeman, San Francisco, 1963.*

[15] *Nelson, R.D., Jr., Lide, D.R., Jr. and Maryott, A.A., NSRDS-NBS10, Sept. 1967.*

We have found it computationally efficient to use an analytic fit for λ_i and η_i. Values for these parameters were generated from equations (19) and (20), respectively. The temperature range was 300-3000K and evaluations were made at 100K intervals. The functional form AT^B was then fitted to these data in a least squares sense. The coefficients A and B for each species and the overall rms error of each fit is listed in Table 6. Table 7 lists the species thermal conductivities at 2000K.

The binary diffusion coefficients[13] are generated from the expression

$$pD_{ij}(cm^2s^{-1}atmos^{-1}) = 1.858 \times 10^{-3}T^{3/2}[(M_i+M_j)\ (M_iM_j)^{-1}]^{\frac{1}{2}}/\sigma_{ij}^2\Omega^{(1,1)}(T^*_{ij}) \tag{22}$$

where $T^*_{ij} \equiv (\varepsilon/k)^{-1}_{ij}\ T$. For non-polar, non-polar interactions the combining laws are $\varepsilon_{ij} = (\varepsilon_i\varepsilon_j)^{\frac{1}{2}}$ (23)

and

$$\sigma_{ij} = \tfrac{1}{2}(\sigma_i + \sigma_j). \tag{24}$$

For polar, non-polar interactions we employ the modified combining laws:

$$\sigma_{np} = (\sigma_n + \sigma_p)\ \xi^{-1/6} \tag{25}$$

and

$$\varepsilon_{np} = (\varepsilon_n\varepsilon_p)^{\frac{1}{2}}\xi^2 \tag{26}$$

where

$$\xi = 1 + 2^{-\frac{1}{2}}\ (\alpha_n t^*_p/\sigma_n^3)\ [\varepsilon_p/\varepsilon_n]^{\frac{1}{2}} \tag{27}$$

and

$$t_p^* = 8^{-\frac{1}{2}}\ \mu_p^2/\varepsilon_p\sigma_p^3. \tag{28}$$

We note in passing that $2\delta = t_p^*$. To evaluate equation (27) we need to specify the polarizability of the non-polar molecule, α_n. For H_2, O_2 and N_2, α_n (in units of 10^{-24} cm^3) is[16]: 0.79, 1.60 and 1.76, respectively.

The values of the D_{ij} are computed at 100K intervals over the temperature range 300-3000K by means of Eq. (22) and, as the values for λ_i, are fitted to the convenient functional form AT^B. The coefficients A and B and the overall error of the fit (in an rms sense) are given in Table 8.

Some of these values can be checked against experimental data and other D_{ij} determinations. Table 9 shows values of D_{ij} computed from the parameters listed in Table 8 and experimental data taken at 273K and one atmosphere pressure. We find this agreement good to excellant.

---

[16] *Ref. 13, Table II-2, p. 529.*

TABLE 6. COEFFICIENTS FOR THE VISCOSITY AND HEAT CONDUCTIVITY EXPRESSIONS IN THE FORM AT^B. RELATIVE ERROR EXPRESSES ROOT-MEAN-SQUARE DEVIATION OF THE FIT.

	Viscosity (η_i)			Thermal Conductivity (λ_i)		
	A	B	Rel Error	A	B	Rel Error
	($X10^{-6}$ gms^{-1}cm^{-1})	($X10^{-1}$)	(%)	($X10^{-6}$ cals^{-1}cm^{-1}K^{-1}	($X10^{-1}$)	(%)
H	2.528	6.7349	1.4	16.043	6.7349	1.4
OH	4.5964	6.6721	1.1	1.4149	7.6786	1.0
O	4.4592	6.6721	1.1	2.2550	6.5670	0.7
HO_2	4.8636	6.6773	1.1	0.6194	8.4793	2.6
H_2	2.2054	6.4915	0.2	5.3754	7.5830	2.1
O_2	4.7893	6.6773	1.1	0.7616	7.8274	1.4
H_2O	0.4856	9.5230	3.1	0.0769	11.767	2.5
N_2	4.3526	6.5835	0.6	0.8030	7.6476	0.7

TABLE 7. THERMAL CONDUCTIVITY AT 2000K.
(computed from Table 6)

Species	λ_i / cal-cm^{-1}-K^{-1}s^{-1}	λ_i / (W/mK)
H	$2.6822 * 10^{-3}$	1.122
OH	$4.847 * 10^{-4}$	0.2028
O	$3.318 * 10^{-4}$	0.1388
HO_2	$3.900 * 10^{-4}$	0.1632
H_2	$1.712 * 10^{-3}$	0.7163
O_2	$2.921 * 10^{-4}$	0.1222
H_2O	$5.892 * 10^{-4}$	0.2465
N_2	$2.687 * 10^{-4}$	0.1124

Table 10 shows the expressions of Marrero and Mason[17] for selected D_{ij}, also in the form AT^B. Their expressions are based upon data (except for H_2-N_2) and they rate the quality of their fits in the following order:

H_2O - N_2 ± 4%

H_2O - O_2 ± 7%

H - H_2 ± 5% (300°K); ± 30% (>1000K)

H-N_2, O-N_2, O-O_2 ± 10%(300K); ± 25%(>1000K).

The last column of Table 10 shows the comparison of their values with the ones generated from the parameters listed in Table 8. This comparison is made over the interval 300 $\leq T \leq$ 3000K except where noted. Comparisons for the major species are within 13% (rms). The O-N_2 and O-O_2 show larger rms deviations but their effects on flame speed and profiles is expected to be small.

[17] *Marrero, T.R. and Mason, E.A., J.Phys. Chem. Ref. Data 1, 3-118, 1972.*

Table 8. ANALYTIC FIT OF FORM AT^B TO THE BINARY DIFFUSION COEFFICIENTS D_{ij}

pD_{ij}		A	B	Error
i	j	($X10^{-4}cm^2s^{-1}atm^{-1}$)		(%)
H	H	2.1700	1.6846	1.3
H	OH	1.0997	1.6815	1.2
H	O	1.1016	1.6815	1.2
H	HO_2	0.91865	1.6818	1.2
H	H_2	1.6560	1.6649	0.4
H	O_2	0.91907	1.6818	1.2
H	H_2O	0.6409	1.7525	2.7
H	N_2	0.90158	1.6758	0.9
OH	OH	0.27234	1.6786	1.1
OH	O	0.27656	1.6786	1.1
OH	HO_2	0.20564	1.6788	1.1
OH	H_2	0.73760	1.6640	0.3
OH	O_2	0.20673	1.6788	1.1
OH	H_2O	0.16361	1.7437	2.6
OH	N_2	0.20894	1.6734	0.8
O	O	0.28072	1.6786	1.1
O	HO_2	0.20984	1.6788	1.1
O	H_2	0.74002	1.664	0.3
O	O_2	0.21091	1.6788	1.1
O	H_2O	0.16622	1.7437	2.6
O	N_2	0.21296	1.6734	0.8
HO_2	HO_2	0.14846	1.6791	1.1
HO_2	H_2	0.62386	1.6641	0.3
HO_2	O_2	0.14961	1.6791	1.1
HO_2	H_2O	0.12144	1.7445	2.6

Table 8. ANALYTIC FIT OF FORM AT^B TO THE BINARY DIFFUSION COEFFICIENTS D_{ij} (cont'd).

pD_{ij}		A	B	Error
i	j	($X10^{-4}cm^2s^{-1}atm^{-1}$)		(%)
HO_2	N_2	0.15364	1.6736	0.8
H_2	H_2	1.1299	1.6600	0.2
H_2	O_2	0.62442	1.6641	0.3
H_2	H_2O	0.58694	1.6937	1.7
H_2	N_2	0.59990	1.6627	0.3
O_2	O_2	0.15076	1.6791	1.1
O_2	H_2O	0.10965	1.7585	2.8
O_2	N_2	0.15474	1.6736	0.8
H_2O	H_2O	0.026558	1.9523	3.1
H_2O	N_2	0.12198	1.7403	2.5
N_2	N_2	0.15678	1.6700	0.6

Note: The logarithmic weighting of these fits was taken into account. See R.J. Cvetanovic and D.L. Singleton, Int., J. Chem. Kinet. 9, 481-488, 1977 and 9, 1007-1009, 1977.

TABLE 9. COMPARISON OF THE VALUES OF SELECTED D_{ij} FROM TABLE 8 COMPUTED AT 1 atmos. and 273K WITH EXPERIMENTAL DATA

Species pair	AT^B	D_{exp}*
H_2 - N_2	0.674	0.674
H_2 - H_2O	0.784	0.759
O_2 - H_2O	0.211	0.214
H_2 - O_2	0.750	0.701
N_2 - H_2O	0.212	0.212
N_2 - O_2	0.185	0.181
H - H_2	1.88	1.86
O - O_2	0.259	0.281
H - N_2	1.09	0.945
O - N_2	0.254	0281
H_2 - H_2	1.25	1.26
O_2 - O_2	0.186	0.184
N_2 - N_2	0.184	0.180

*D_{exp} (T = 273, p = 1 atmos) from: Warnatz, J. Ber Bunsenges. Phys Chem 82 643-649, 1978, Table 2.

TABLE 10. COMPARISON OF SELECTED D_{ij} WITH THOSE OF MARRERO AND MASON[17]

D_{ij}		$10^5 A$(atmo-cm^2)	B	Temperature Range (K)	Comparison With Values from Table 8
i	j				
H_2	O_2	4.17	1.732	252-10^4	9.8%
N_2	O_2	1.13	1.724	285-10^4	6.0%
N_2	H_2O	0.187	2.072	282-373	1.7% (300K only)
O_2	H_2O	0.189	2.072	282-450	12.9% (300-500)
		2.78	1.632	450-1070	10.6% (500-1100)
H	H_2	11.3	1.728	190-10^4	8.5%
O	N_2	1.32	1.774	280-10^4	25.7%
O	O_2	1.32	1.774	280-10^4	22.8%
H_2	N_2	*	*	65-10^4	12.2%

$$*\ell n(pD_{H_2N_2}) = \ell n\, A + s\, \ell nT - \ell n[\ell n(\phi_o/kT)]^2 - (S/T) - (S'/T^2)$$

where

$10^3 A = 15.39$ atmos-cm^2[s(K)^5]$^{-1}$

$s = 1.548$

$10^{-8}\phi_o/k = 0.316$

$S = -2.80$

$S' = 1067.$

The LJ parameters for D_{H_2}-N_2 were determined from the empirical combining rules Eqs. (23) and (24) for H_2 and N_2.[17]

Table 11 shows the results of comparisons of the viscosity and thermal conductivity as computed from the parameters on Table 6 and the data listed by Touloukian et al[18,19]. The large deviation for λ_{H_2O} suggests that a fit could be made to the data themselves.

TABLE 11. COMPARISON OF THERMAL CONDUCTIVITY AND VISCOSITY WITH DATA OF Touloukian et al.[18,19]

Species	λ deviations	Temperature Range (K)	η deviations	Temperature Range (K)
H_2	+ 4.7%	300-2000	4.90	300-2000
N_2	- 3.6%	300-3000	1.34	300-2000
O_2	+ 1.1%	300-1500	3.03	300-2000
H_2O	- 29.8%	300-900	4.13	300-1000

+ = data > computation

Multispecies Transport

Once the λ_i and D_{ij} are determined, as above, there remains to assemble the thermal conductivity of the mixture and decide how to handle the multi-species diffusion.

Although some rather involved formulations are available in the literature[18] to determine λ_{mix}, we have found[20] that the values from these expressions differ little from the expression

$$\lambda_{mix} = 0.5 \{\Sigma_i X_i\lambda_i + (\Sigma_i X_i/\lambda_i)^{-1}\} . \quad (29)$$

For the diffusion transport parameters[21] we employ a generalization of Fick's Law, namely

[18] *Touloukian, Y.S., Liley, P.E. and Saxena, S.C., Thermal Conductivity (non-metallic Liquids and Gases), IFI/Plenum, N.Y., 1970.*

[19] *Touloukian, Y.S., Saxena, S.C. and Hestermans, P. Viscosity. IFI/Plenum, N.Y., 1975.*

[20] *Coffee, T.P. and Heimerl, J.M., Combustion and Flame 43, 273-289 (1981) and BRL Tech. Report ARBRL-TR-02302, Mar. 81.*

[21] *This is the so-called Method V considered in Ref. 20. Method VI is considered in the Appendix.*

$$Y_i V_i = - D_{im} (Y_i)_x \tag{30}$$

where

$$D_{im} = (1-X_i)(\Sigma_{j \neq i} X_i / D_{ij})^{-1}. \tag{31}$$

Again we have found[20] little difference in the computed flame speeds, species profiles or temperature profiles using this generalized Fick's law vs. more complex formulations that solve for the diffusion velocity (such as the Stefan-Maxwell equations do).

We have further noted that in the Lennard-Jones formalism

$$D_{ij} \propto T^{1.5}/\Omega^{(1,1)}. \tag{32}$$

Now $\Omega^{(1,1)} \propto T^{-0.17}$ and since $\rho \propto T^{-1}$ we see that $\rho^2 D_{ij}$ is nearly independent of temperature. Generalizing we assume that $\rho^2 D_{im}$ is constant. Likewise for a monatomic gas $\lambda \propto T^{\frac{1}{2}}/\Omega^{(2,2)}$, where $\Omega^{(2,2)} \propto T^{-0.16}$. It is thus reasonable to assume that $\rho\lambda$ is independent of temperature.

We now outline a procedure that permits an a priori selection of these quantities.

For a given flame we know T_u and Y_{iu}, the temperature and the mass fraction of the unburnt mixture. We also know the kinetic scheme, the specific heats and the specific enthalpies. Since enthalpy is conserved, i.e.,

$$\sum_{i=1}^{N} Y_i h_{i_B} = \sum_{i=1}^{N} Y_i h_{i_u}, \tag{33}$$

we can compute the adiabatic flame temperature T_B, as well as the mass fractions of the burnt mixture, Y_{iB}. The numerical procedure is to guess a trial temperature T_t and, using an ODE package, find the corresponding equilibrium mass fractions Y_{it}. We then compute the enthalpy of the burnt mixture and compare with the unburnt mixture enthalpy. T_t is iteratively adjusted until the burned and unburned mixture enthalpies agree to within a predetermined error tolerance. We then accept these values of T_t and Y_{iB}.

As a heuristic rule we select

$$T = 0.5(T_B - T_u) \tag{34a}$$

and

$$Y_i = 0.5\ (Y_{iB} + Y_{iu}) \tag{34b}$$

then evaluate D_{im} and λ_i from Eqs. (31) and (29) respectively. Then $\rho^2 D_{im}$, i = 1,2...N-1 and $\rho\lambda_i$ are evaluated. The diffusion velocity V_N is found from the constraint on the diffusive mass flux that

$$\Sigma Y_i V_i = 0 . \tag{35}$$

At this level of approximation we find it convenient to employ a constant or global c_p. So we assume $c_{pi} = c_p$ = constant for all i. Then the relation

$$h_i = h_i^o + \int_{T_0}^{T} c_{pi}\, dT \tag{36}$$

becomes

$$h_i = h_i^o + c_p(T - T_o) \quad \text{and} \tag{37}$$

the mixture enthalpy is given by

$$\Sigma\, Y_i h_i = \Sigma\, Y_i h_i^o + c_p(T-T_o). \tag{38}$$

Substituting this expression into Eq. (33) we find

$$c_p = \frac{\Sigma\, h_i^o (Y_{iu} - Y_{iB})}{T_B - T_u} . \tag{39}$$

The values used here are found in Table 12 and yield an average c_p = 3.65×10^{-1} cal-mole^{-1}K^{-1}. We also find that $\rho(T = 1344K) = 2.0364 \times 10^{-4}$ gm cm^{-3}, and that T_B = 2390K. This value compares well with the NASA-Lewis value[6] of 2383K.

Table 13 shows the D_i, evaluated at T = 2000K as required for use in the workshop comparisons; the values at the mean temperature, T = 1344K, are included for completeness.

Table 14 contains values of λ_i and D_{im}, both at 1344K, used in the computation of $\rho^2 D_{im}$ and $\rho\lambda_{mix}$. The value of this density at 1344, given above, was computed from $\rho = \rho/(RT\Sigma Y_i/M_i)$; the mass fractions, Y_i, are taken from Table 12 (ie., Y_{1344}); and λ_{mix} is composed from Eq. (29). This equation requires the species mole fractions and these are computed from the standard relation: $X_i = (Y_i/M_i)/(\Sigma Y_j/M_j)$. The values for $\rho^2 D_{im}$ used in the flame code are listed in the last column of Table 14. The value found for λ_{mix} is 3.29×10^{-4}cal-s^{-1}-cm^{-1}-K^{-1} and so the value for $\rho\lambda_{mix}$ used in the flame code is 6.70×10^{-8} gm-cal-cm^{-2}-s^{-1}-K^{-1}.

The workshop had requested values for λ_{mix} at 2000K. Table 15 contains a listing of the values for Y_i at 2000K taken from the flame code output. Also listed are the values of the corresponding mole fractions. This information, the values of λ_i from Table 6 and Eq. (29) were used to complete λ_{mix} = 4.44×10^{-4} cal-s^{-1}-K^{-1} (i.e. 0.1857 W $m^{-1}K^{-1}$).

TABLE 12. PARAMETERS NEEDED TO DETERMINE DIFFUSION TRANSPORT PARAMETERS, EQUATIONS (31) and (39)

	Y_u	Y_B	Y_{1344}	h^o (cal/gm)
H	*	7.517(-5)	3.759(-5)	5.21(+4)
OH	*	5.081(-3)	2.541(-3)	5.58(+2)
O	*	4.059(-4)	2.030(-4)	3.72(+3)
HO_2	*	9.475(-7)	4.738(-7)	1.51(+2)
H_2	2.830(-2)	1.212(-3)	1.476(-2)	-1.60(-1)
O_2	2.264(-1)	7.504(-3)	1.170(-1)	-3.57(-2)
H_2O	*	2.404(-1)	1.202(-1)	-2.21(+3)
N_2	7.4528(-1)	7.453(-1)	7.453(-1)	-3.95(-2)
T(°K)	298	2390	1344.	

*Values are machine zero.

TABLE 13. EVALUATION OF D_{ij} AT T = 1344K and 2000K

i	j	D_{ij}(T = 1344°K) cm^2-s^{-1}	D_{ij}(T = 2000K) cm^2-s^{-1}
H	OH	20.03	39.08
H	O	20.07	39.15
H	HO_2	16.77	32.72
H	H_2	26.76	51.87
H	O_2	16.78	32.74
H	H_2O	19.87	39.87
H	N_2	15.76	30.68
OH	O	4.93	9.61
OH	HO_2	3.67	7.16
OH	H_2	11.84	22.95
OH	O_2	3.69	7.20
OH	H_2O	4.66	9.33
OH	N_2	3.59	6.98
O	HO_2	3.74	7.31
O	H_2	11.88	23.02
O	O_2	37.68	7.34
O	H_2O	47.39	9.48
O	N_2	36.59	7.11
HO_2	H_2	10.02	19.42
HO_2	O_2	2.68	5.22
HO_2	H_2O	3.48	6.97
HO_2	N_2	2.64	5.14
H_2	O_2	10.03	19.44
H_2	H_2O	11.67	22.88
H_2	N_2	9.54	18.48
O_2	H_2O	3.48	6.70
O_2	N_2	2.66	5.18
H_2O	N_2	3.39	6.78

TABLE 14. THE TRANSPORT PARAMETERS AT THE MEAN TEMPERATURES, T=1344K

Species	λ_i / $X10^{-4}$ cal-s^{-1}-cm^{-1}-K^{-1}	D_{im} / cm^2-s^{-1}	$\rho^2 D_{im}$ / $x10^{-7}$ gm^2-cm^{-4}-s^{-1}
H	20.52	17.61	7.30
OH	3.57	4.24	1.76
O	2.56	4.32	1.79
HO_2	2.78	3.15	1.31
H_2	12.67	9.93	4.12
O_2	2.14	3.21	1.33
H_2O	3.69	3.95	1.64
N_2	1.98	4.30	1.78

TABLE 15. FLAME CODE VALUES OF Y_i AND X_i AT T=2000K

Species	M_i	Y_i	X_i
H	1	7.79(-4)	1.84(-2)
OH	17	1.00(-2)	1.39(-2)
O	16	3.54(-3)	5.22(-3)
HO_2	33	9.37(-6)	6.70(-6)
H_2	2	3.08(-3)	3.63(-2)
O_2	32	2.38(-2)	1.76(-2)
H_2O	18	2.14(-1)	2.81(-1)
N_2	28	7.45(-1)	6.28(-1)

V. Results and Discussion

The results requested in the B problem are the flame velocity and the maximum values of the mass fraction profiles of H, O, OH, and HO_2 and the maximum and minimum values of the enthalpy. The mixture enthalpy profile is computed from the other known functions. Specifically,

$$h_{mix} = \sum_{i=1}^{N} Y_i h_i \tag{40}$$

which for transport method 5 with constant c_p reduces to

$$h_{mix} = \sum_{i=1}^{N} Y_i h_i^{o} + c_p(T-T_o). \tag{41}$$

Since the functions $Y_i(x)$ and $T(x)$ are known $h_{mix}(x)$ can be generated.

The flame speeds are shown in Table 16. The first column contains the values predicted by the code using the nominal values of ψ_5, ε and NINT. The second column shows the values predicted when the burned end numerical boundary ψ_R, the temporal error criterion, ε, and the number of breakpoints NINT are simultaneously changed. The third column shows the flame speed predictions from the same code and input parameters except that the kinetics of Dixon-Lewis[9] are used.

Since our grid[7] adapts to the temperature profile, the flame speed from this profile is the most accurate. All other determinations agree within 5% except the HO_2 profile. The reason for this exception is that the interval of integration is taken from the cold boundary to approximately the mid-point of ψ-space (see Eq. (9)). The HO_2 profile (see Fig. 1) is a sharp "spike" that occurs within the integration interval and so the flame speed determination is expected to be grossly in error. This has been checked by raising NCN from six to twelve and simultaneously lowering ψ_5 to 2.0. The former extends the region of detail about the inflection of the temperature profile and the latter decreases the spatial resolution. In this case the flame velocity predicted for the HO_2 profile was 150 cm-s^{-1} showing the expected trend. In addition the flame speed predicted for the OH profile was 197 cm-s^{-1} and all other determinations changed by 3 units or less.

All these results are in good agreement with the computed flame velocity of 200 cm-s^{-1} (Dixon-Lewis[9] his figure 40). The corresponding measurements[9] show relatively wide scatter; i.e., 187-280 cm-s^{-1}.

Since the numerical range of ψ space is finite, we need to check the adequacy of our selection of the value of this numerical boundary. If this range is too small, mass or heat or both will "leak" out.

The mass and heat flux fractions are defined

$$\varepsilon_k = Y_k + \rho Y_k V_k (\rho u)^{-1} \tag{42}$$

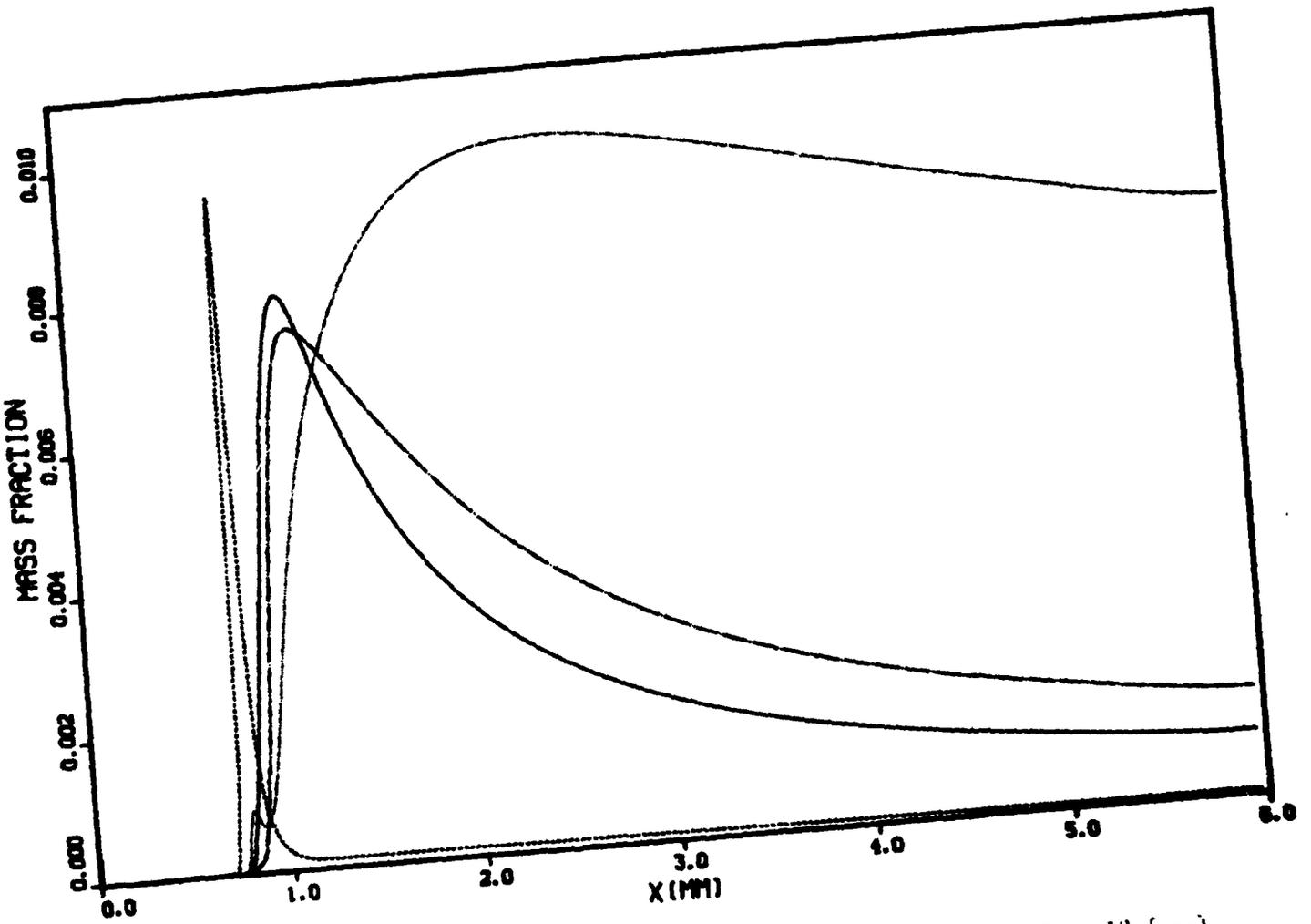

Fig. 1 Radical species mass fraction profiles; Hx3 (-), OH (...), O (-.-.) and HO_2 x 12 (---). Transport method 5.

TABLE 16. COMPUTED FLAME SPEEDS

Variable	Flame[a] Velocity cm-s^{-1}	Flame[b] Velocity cm-s^{-1}	Flame[c] Velocity cm-s^{-1}
Temp	200	200	217
H	199	200	216
OH	196	190	214
O	195	197	215
HO_2	-1300	-229	121
H_2	199	200	216
O_2	199	199	216
H_2O	199	199	216
N_2	197	198	216

[a] $\psi_5 = 2.9$, $\varepsilon = 3\text{x}10^{-5}$, NINT = 24, NCN = 6, FC = 6.

[b] $\psi_5 = 3.3$, $\varepsilon = 10^{-5}$, NINT = 30, NCN = 6, FC = 6 (check)

[c] Dixon-Lewis Kinetics[9] $\psi_5 = 0.8$, $\varepsilon = 3\text{x}10^{-4}$, NINT = 16, NCN = 6, FC = 8.0.

---

and

$$\varepsilon = T_u + \lambda(T)_x \, c_p^{-1} \, (\rho u)^{-1}, \tag{43}$$

respectively. Since V_K is always related to the derivative $(Y_K)_x$ and in the Fick's law case, considered here, (42) can be written

$$\varepsilon_K = Y_K - \rho D_{im} (Y_K)_x \, (\rho u)^{-1} \, . \tag{44}$$

We see that if the derivatives $(Y_K)_x = (T)_x = 0$ at the cold boundary then the flux fraction should equal the originally assigned values of $Y_{k\bar{a}}$ and T_u. We find the derivatives to be all $\leq 10^{-7}$ and that the values of the flux fractions are identical to the cold boundary values to at least five significant figures.

Table 17 shows the requested peaks for the Peters B problem. These are determined from the output routines which typically contain ∿ 200 data points per profile. These in turn have been generated from the 40 collocation points and the known coefficients of the B-spline functions.

Mass fraction profiles of the minor (OH, O, H and HO_2) and major (H_2, O_2, H_2O and N_2) species can be found in figures 1 and 2, respectively. Figure 3 shows the profiles of temperature and enthalpy. The most interesting of these profiles are those of HO_2 and OH. The fact that the HO_2 peak lies close to the smaller OH peak suggests that they may be related. Let us first examine what is happening to form the HO_2 peak.

TABLE 17. PEAK VALUES OF RADICALS AND EXTREMA OF ENTHALPY

i	$Y_{i\ max}$	Location (mm)	Temp (K)
H	2.6740E-3	1.0935	1353.8
OH	1.0012E-2	2.4838	1968.6
O	7.5460E-3	1.1399	1408.9
HO_2	7.9263E-4	0.78185	369.0
max enthalpy	8.7725E+1*	0.90429	916.9
min enthalpy	-2.2690E+1*	1.2143	1479.5

*units of cal/gm.

The only source of HO_2 in this region is the reaction

$$H + O_2 + M \rightarrow HO_2 + M \ . \qquad \text{(R7)}$$

H is transported toward the cold boundary by diffusion and, before the flame front, O_2 is in abundant supply. So HO_2 builds up to the HO_2 peak near 0.76 mm until the reactions

$$HO_2 + H \rightarrow 2OH \qquad \text{(R8)}$$

$$HO_2 + H \rightarrow H_2 + O_2 \qquad \text{(R9)}$$

and

$$HO_2 + OH \rightarrow H_2O + O_2 \qquad \text{(R10)}$$

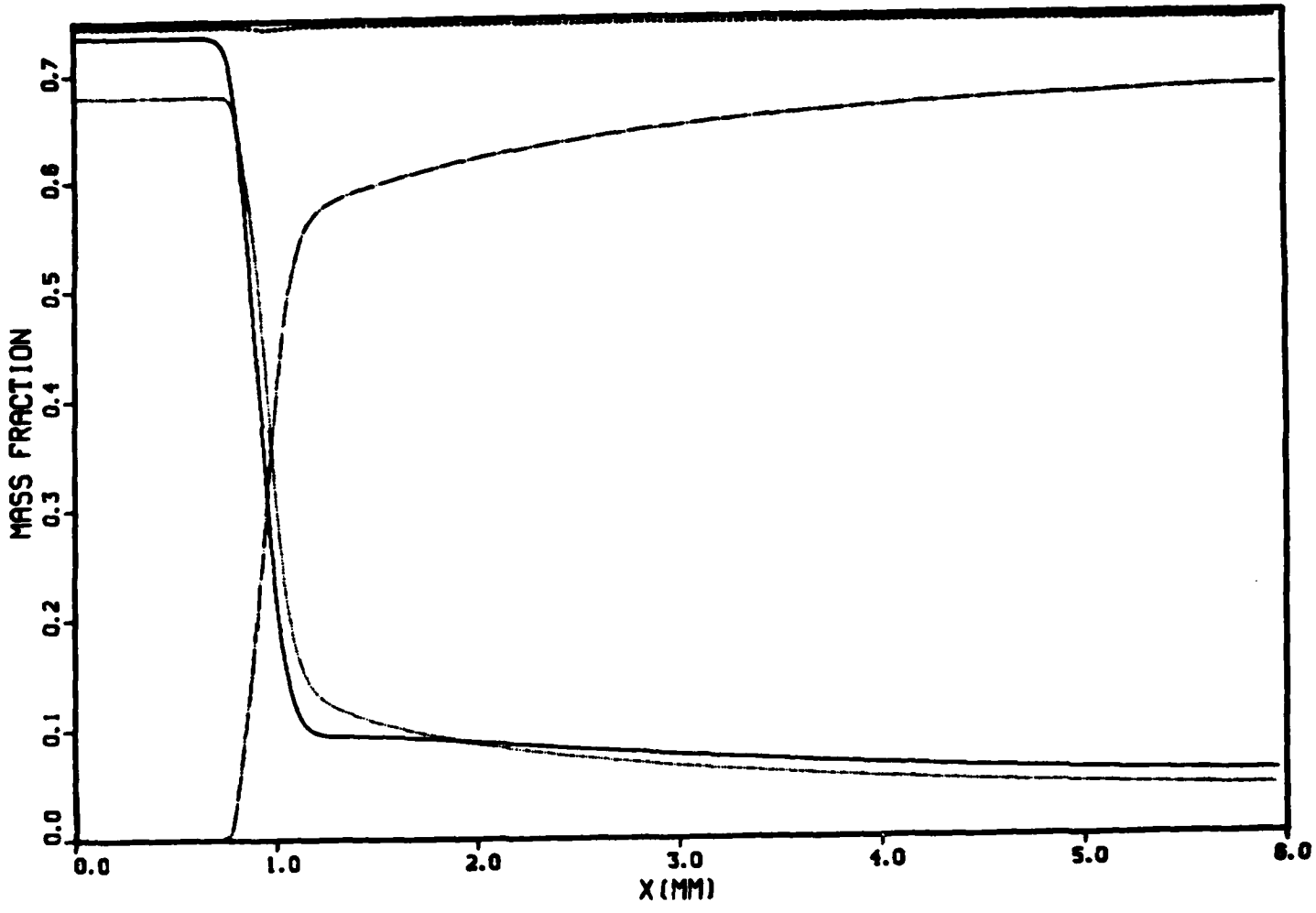

Fig. 2 *Major species mass fraction profiles;* H_2 x 26 (—), O_2 x 3 (...), H_2O x 3 (-.-.) and N_2 (---). Transport method 5.

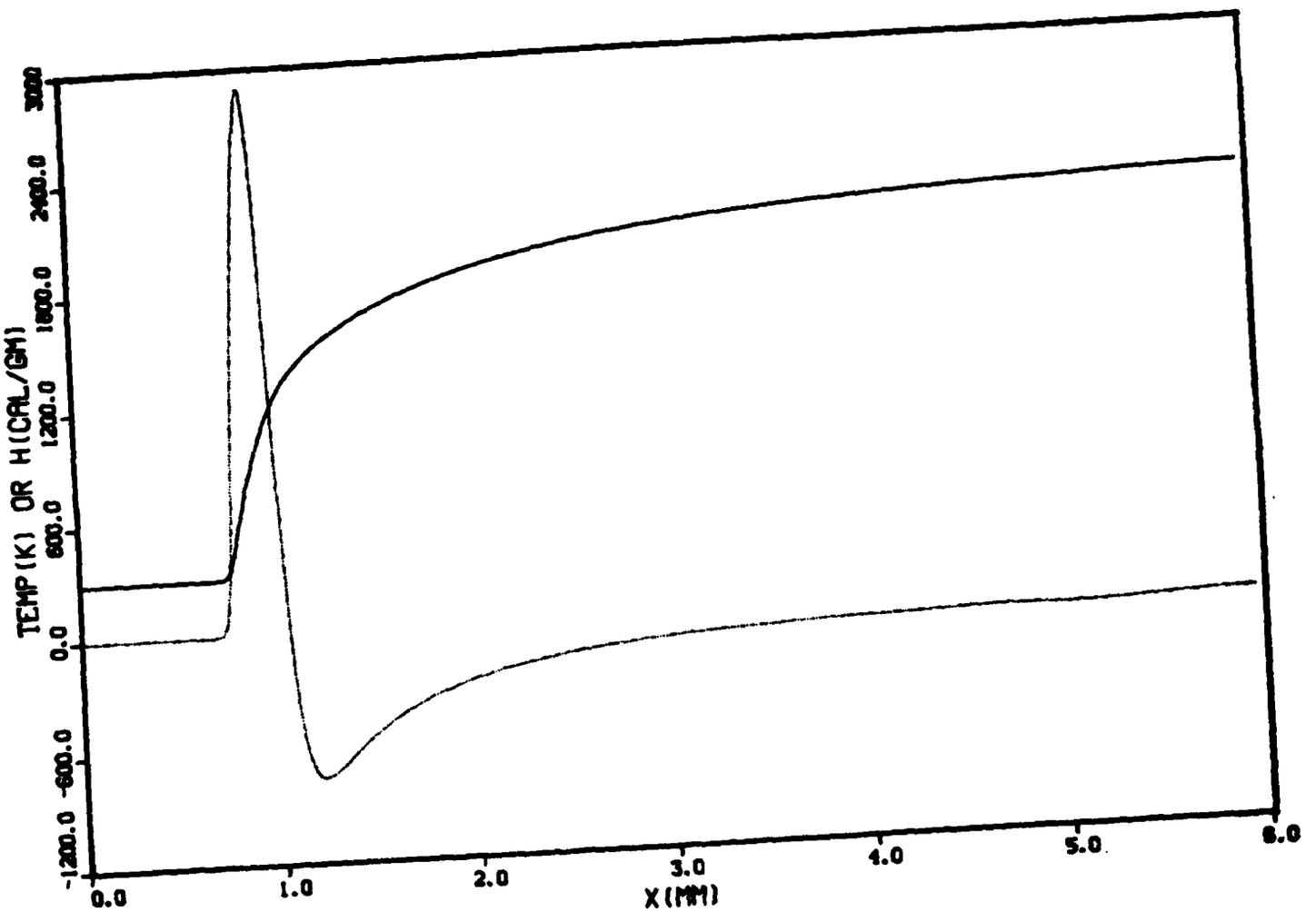

Fig. 3 Temperature and enthalpy profiles; Temperature (-) and enthalpy x 33 (...). Transport method 5.

are significant and together dominate the HO_2 loss. (Small but non-negligible losses to the HO_2 concentration also occur through diffusion and conduction.) The temperature rises sufficiently till the rate of these HO_2 loss mechanisms exceed the rate of HO_2 production and Y_{HO_2} is observed to fall.

The smaller OH peak (near 0.8 mm) is caused by the following mechanism.

The major source of OH is reaction 8 (which also depletes HO_2); the major OH sink is

$$H_2 + OH \rightarrow H_2O + H, \tag{R1}$$

but the OH profile tends to track the HO_2 profile except that near 0.9 mm the chain branching reactions

$$O_2 + H \rightarrow O + OH \tag{R2}$$

$$H_2 + O \rightarrow H + OH \tag{R3}$$

become important. With increasing temperature the OH builds up again. The gap in the Y_{OH} profile is the location where OH is tracking HO_2 and reactions (R2) and (R3) do not have significant influence.

In Figure 4 we see a plot of X_{N_2} vs. distance. The rise needs to be understood because N_2 is a non-reacting diluent and the corresponding Y_{N_2} plot is flat (see Fig. 2). As we shall now show, this behavior can be accounted for in the Y to X transformation.

Given that $Y_i(A) = Y_i(B) = \ldots$, where A,B,... are spatial locations, we ask what is the relationship between say, $X_i(A)$ and $X_i(B)$. In general

$$X_i(A) = (Y_i(A)/M_i)/(\Sigma\, Y_j(A)/M_j). \tag{45}$$

Then

$$X_i(B) = (Y_i(B)/M_i)/(\Sigma\, Y_j(B)/M_j) \tag{46}$$

$$= (Y_i(A)/M_i)/(\Sigma\, Y_j(B)/M_j) \quad .$$

We require an expression for the denominator of (46) in terms of location A. Since

$$\Sigma\, Y_j(B)/M_j = \sum_{j\neq i} Y_j(B)/M_j + Y_i(B)/M_i$$

and

$$\Sigma\, Y_j(A)/M_j = \sum_{j\neq i} Y_j(A)/M_j + Y_i(A)/M_i \,.$$

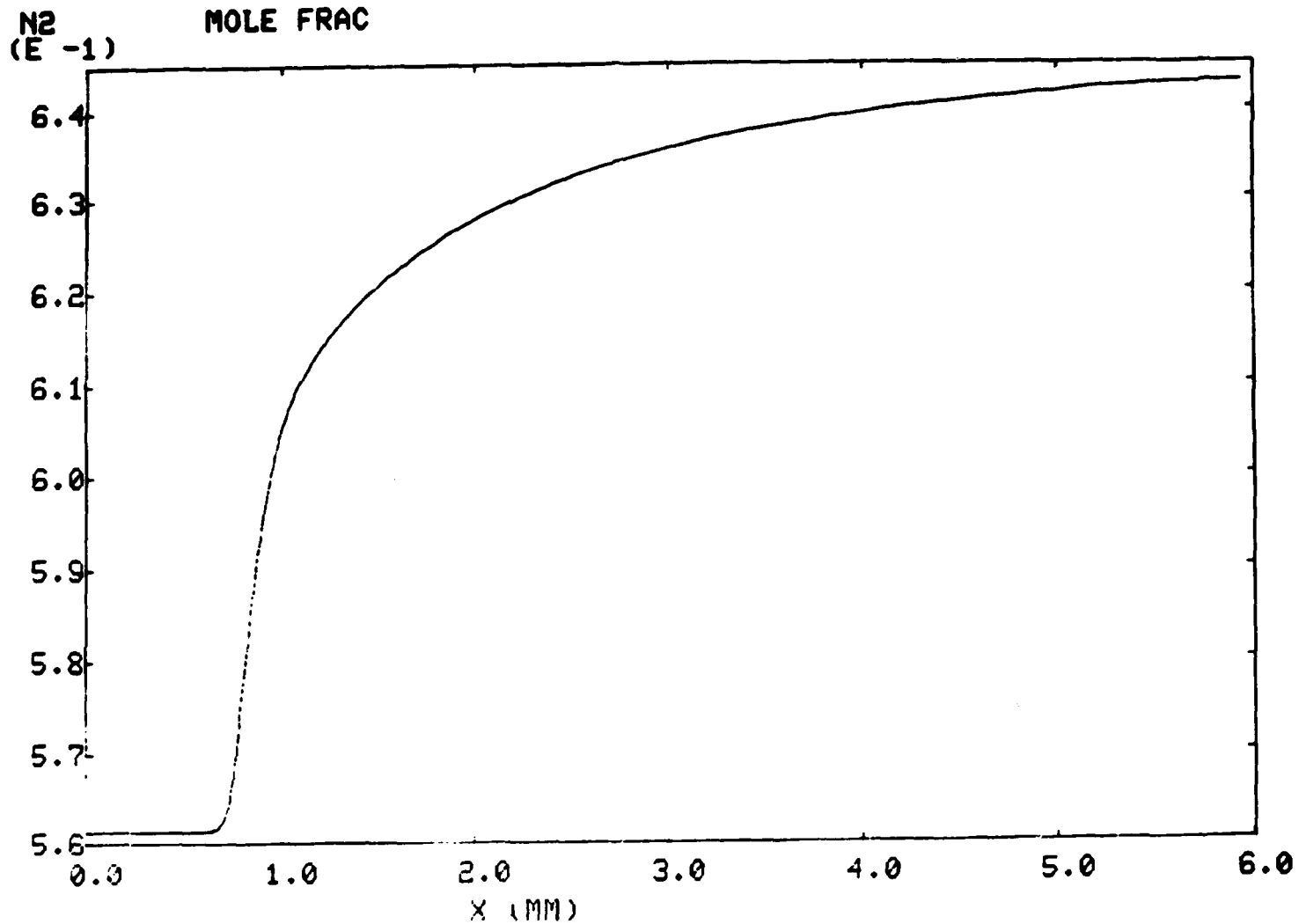

Fig. 4 N_2 mole fraction profile.

We can equate $Y_i(B)$ and $Y_i(A)$ to find that

$$\Sigma\ Y_j(B)/M_j = \sum_{j\neq i} (Y_j(B)-Y_j(A))/M_j + \Sigma\ Y_j(A)/M_j \qquad (47)$$

Substituting (47) into (44) and using (45) we find that

$$X_i(A)/X_i(B) = 1 + \alpha\ , \qquad (48)$$

where $\alpha = \sum_{j\neq i} ((Y_j(B)-Y_j(A))/M_j)/(\Sigma\ Y_j(A)/M_j)$.

Note that if $\alpha << 1$ then $X_i(A) \simeq X_i(B)$; if $\alpha \lesseqgtr 0$ then $X_i(A) \lesseqgtr X_i(B)$. These last inequalities allow the possibility that a flat Y_i profile could be transformed into an X_i profile that is quite different in shape.

As a check, we take the Y_j's from the code output and compute ε (see Eq. 44), for a selected number of collocation points 16 through 21 corresponding to 0.7 mm to 0.8 mm. We use a point in the flat portion of the curve, location 10 ($\sim$ 0.52 mm) as the fiducial or reference point, A. From the code output we can also compute $X_i(A)/X_i(B) - 1$. If nothing but the transformation were involved these values would be identical. Table 18 shows these values. As can be seen the values are quite close; the differences are attributed to transport processes and numerical "slop".
(Recall that Y_{N_2} is computed from $1-\sum_{i}^{N-1} Y_i$.)

Figure 5 shows Y_{O_2} as a function of distance and the expected monatomic decrease. However Figure 6 shows X_{O_2} and a sensible "bump" appears right before the steep slope. Reference to Table 18 shows that at locations 16 & 17 the trend is similar to the Y_{N_2}. However for the higher locations the actual curve, G, departs from the one that only takes into account the Y→X transformation, F. In other words some other process is occurring besides the simple transformation. Examination of the output shows that O_2 diffusion is the major influence on the profile. That reactions play a negligible part in explaining the Y_{O_2} "bump" is consistent with the low temperatures in this region (<500K).

VI. SUMMARY

Besides the requested information we have found several interesting profiles, whose bumps and wiggles could have been attributed to numerical artifacts, but upon closer examination proved to be real for this flame and its input parameters.

In addition, we provide a set of nonkinetic input parameters for this stoichiometeric hydrogen-air flame and compare these values against known experimental determinations. Finally, we show in the Appendix that the multi-species transport algorithm is not important unless one is considering radical profile accuracies of $\sim$20% or less. We also show that the major differences between the two algorithms employed can be attributed to the effects of thermal diffusion.

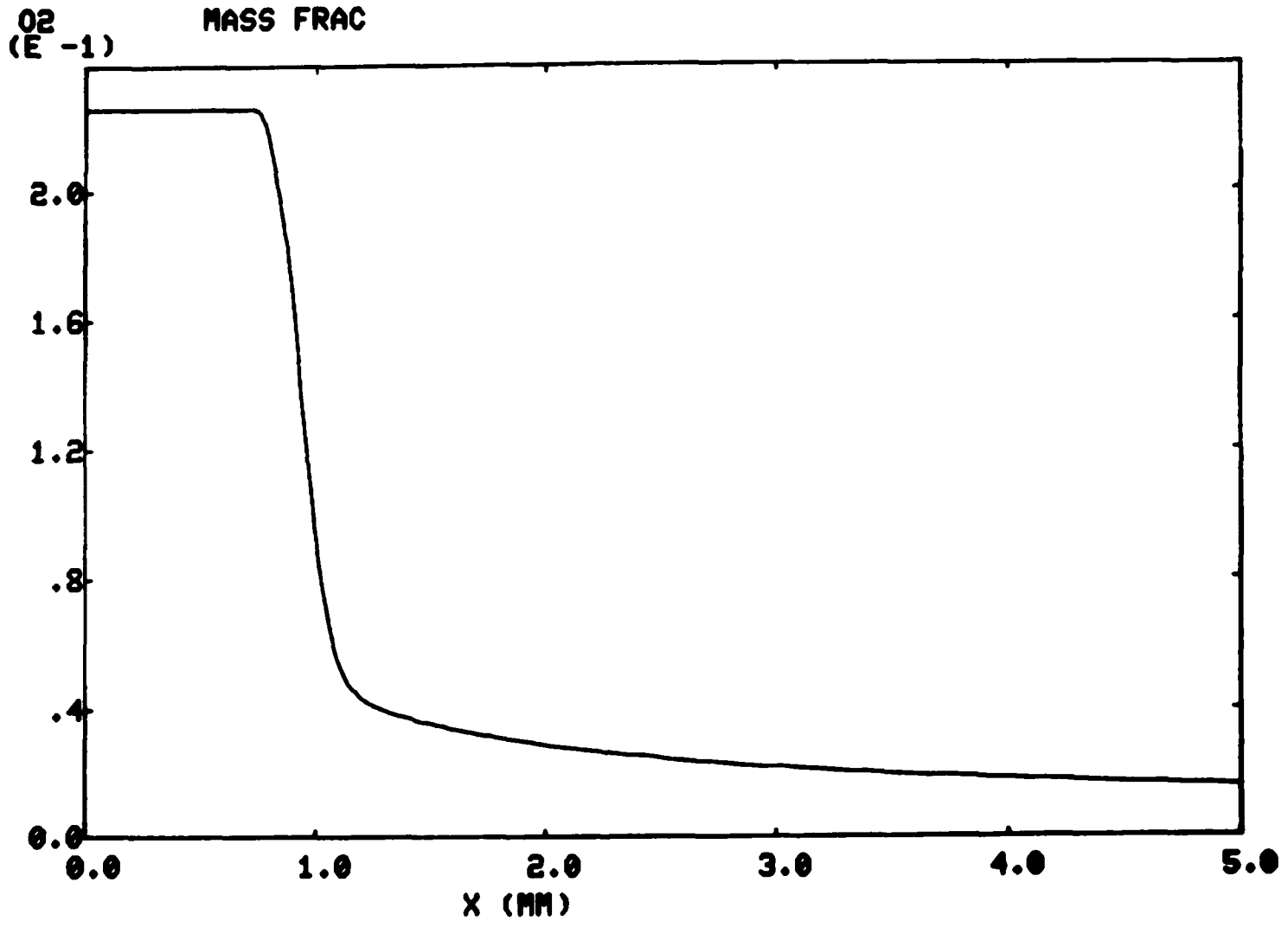

Fig. 5 O_2 mass fraction profile.

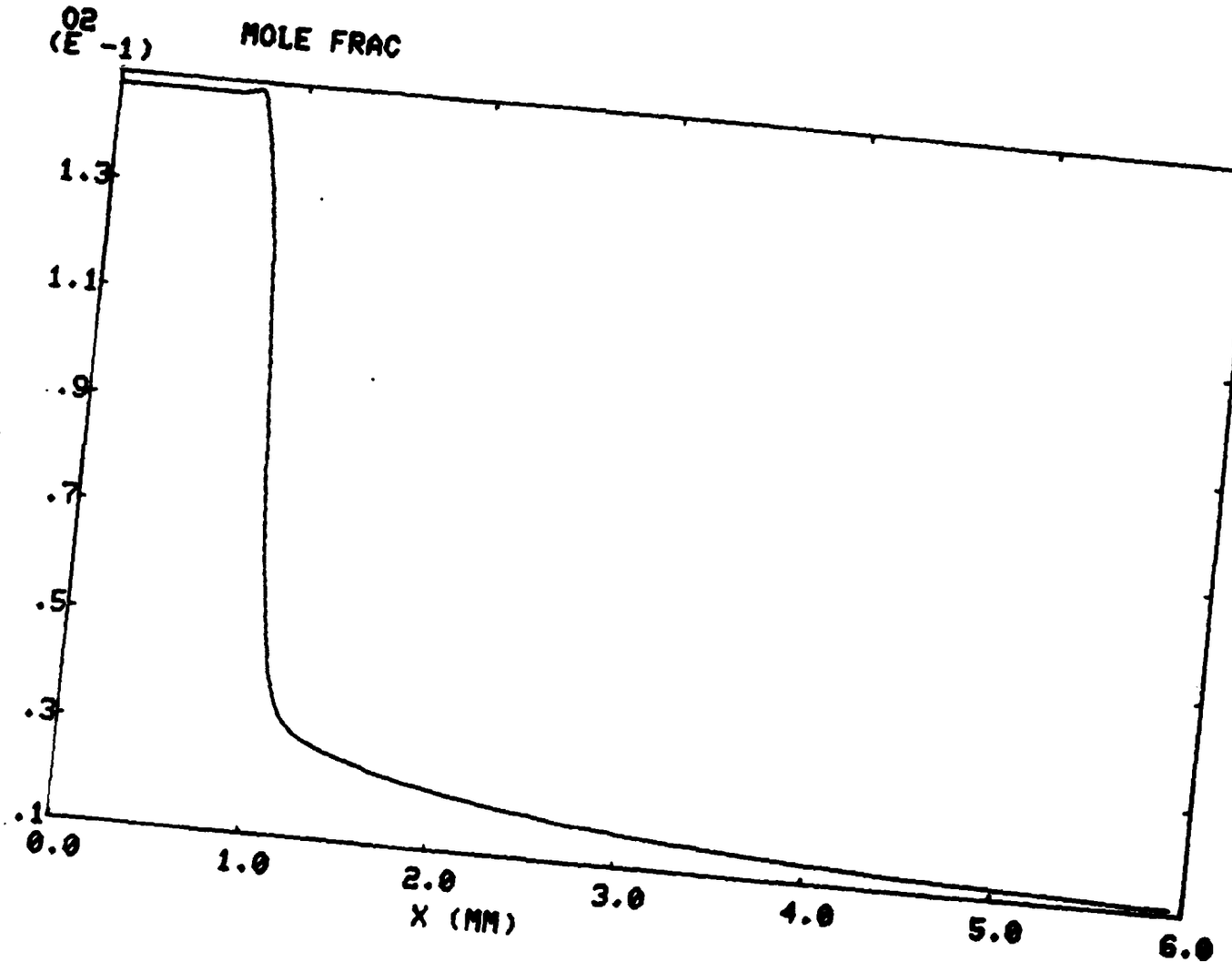

Fig. 6 O_2 mole fraction profile.

TABLE 18. VALUES OF Y↔X TRANSFORMATION AT SPECIFIC LOCATIONS

Location (-B)	$F(N_2,B,10)$	$G(N_2,B,10)$	$F(O_2,B,10)$	$G(O_2,B,10)$
16	-1.80(-3)	-1.90(-3)	-1.66(-3)	-1.62(-3)
17	-4.10(-3)	-4.30(-3)	-3.77(-3)	-3.30(-3)
18	-6.99(-3)	-7.79(-3)	-6.36(-3)	-4.78(-3)
19	-1.28(-2)	-1.31(-2)	-1.12(-2)	-3.91(-3)
20	-1.83(-2)	-1.85(-2)	-1.14(-2)	+3.73(-3)
21	-2.68(-2)	-2.69(-2)	-1.84(-2)	+3.05(-3)

$$F(i,B,A) = \sum_{j \neq i} ((Y_j(B) - Y_j(A)/M_j)/(\Sigma\, Y_j(A)/M_j)$$

$$G(i,B,A) = (X_i(A)/X_i(B)) - 1$$

REFERENCES

1a. Notes on Numerical Fluid Mechanics, Vol. 5, N. Peters and J. Warnatz Ed., Vieweg-Verlag, Pub.

1b. T.P. Coffee, "Flat Flame Olympics: Test Problem A," BRL Report to be published.

1c. Hirschfelder, J.O., Curtiss, C.F. and Bird, R.B., Molecular Theory of Gases and Liquids, 2nd Ed. (corrected with notes), Wiley, New York, 1964.

2. Bird, R.B., Stewart, W.S. and Lightfoot, E.N., Transport Phenomena, Wiley, New York, 1960.

3. Williams, F.A., Combustion Theory, Addison-Wesley, Reading, MA, 1965.

4. Fristrom, R.M. and Westenberg, A.A., Combustion Theory, Addison-Wesley, Reading, MA., 1965.

5. The composition of dry air is by mole %: 78.084 N_2, 20.946 O_2, 0.934 Ar, 0.033 CO_2, 0.003 rare gases. See Matheson Gas Data Book, 5th Ed. by W. Braker and A.L. Mossman, Matheson Gas Products, E. Rutherford, N.J. 1971, p. 9.

6. Gordon, S. and McBride, B.J., Computer Program for Calculation of Complex Chemical Equilibrium Compositions, Rocket Performance, Incident And Reflected Shocks and Chapman-Jouquet Detonations, NASA-SP-273, 1971, (1976 program version).

7. Coffee, T.P. and Heimerl, J.M., BRL Technical Report ARBRL-TR-02212, Jan. 1980. (AD A082803)

8. Coffee, T.P., BRL Memorandum Report to be published.

9. Dixon-Lewis, G., Philos. Trans. Roy. Soc. (London) 292, 45-99, 1979.

10. JANAF Thermochemical Tables, 2nd Ed. By D.R. Stull and H. Prophet, NSRDS-NB37, June 1971.

11. Chase, M.W., Curnutt, J.L., HU, A.J., Prophet, H., Syverud, A.N. and Walker, L.C., J. Chem. Ref. Data 3, 311-480, 1974.

12. Chase, M.W., Curnutt, J.L., Prophet, H., McDonald, R.A. and Syverud, A.N., J. Phys. Chem. Ref. Data, 4, 1-175, 1975.

13. The discussion follows that of Reid, R.C. and Sherwood, T.K., The Properties of Gases and Liquids, 2nd Ed. McGraw-Hill, N.Y., 1966. Viscosity Chap. 9, Thermal Conductivity, Chap. 10 and Diffusion Coefficients, Chap. 11.

14. McCellan, A.L., Tables of Experimental Dipole Moments, Freeman, San Francisco, 1963.

15. Nelson, R.D., Jr., Lide, D.R., Jr. and Maryott, A.A., NSRDS-NBS10, Sept. 1967.

16. Ref. 13, Table 11-2, p. 529.

REFERENCES

17. Marrero, T.R. and Mason, E.A., J. Phys. Chem. Ref. Data 1, 3-118, 1972.

18. Touloukian, Y.S., Liley, P.E. and Saxena, S.C., Thermal Conductivity (non-metallic Liquids and Gases), IFI/Plenum, N.Y., 1970.

19. Touloukian, Y.S., Saxena, S.C. and Hestermans, P. Viscosity. IFI/Plenum, N.Y., 1975.

20. Coffee, T.P. and Heimerl, J.M., Combustion and Flame 43, 273-289 (1981) and BRL Tech, Report ARBRL-TR-02302, Mar. 81. (AD A099735)

21. This is the so-called Method V considered in Ref. 20. Method VI is considered in the Appendix.

22. Warnatz, J. Ber. Bunsenges. Phys. Chem. 82, 643-649 (1978).

APPENDIX A

COMPARISON OF RESULTS USING TRANSPORT METHOD 6

APPENDIX A

Comparison of Results Using Transport Method 6.

In the main body of the text we have employed a mixing algorithm which is based upon Equations (29), (30) and (39). This method, our so-called method 5,[20] consists of a simple definition for λ_{mix}, Eq. (29), and a generalization of Fick's Law plus the selection of constants for $\rho^2 D_{im}$, $\rho\lambda$ and c_p. In order to check the effects of this rather simple mixing algorithm we employed our so-called method 6. This method also used Eq. (29) as the definition of λ_{mix} but accounts for the diffusion velocity by solving a modified form of the Stefan-Maxwell equations. In this method the transport coefficients are temperature dependent. This method also crudely accounts for thermal diffusion. We have assumed that only H and H_2 have non-zero thermal diffusion coefficients. Futher details are given in Ref. 20. All other parameters remain the same.

Table A-1 shows the computed flame speed for both the "Peters B" kinetic listed in Table 1 and the Dixon-Lewis kinetics listed in Table 2. These values are about 4% greater than those in Table 16. The exceptions are for HO_2 whose difficulties we have discussed above and for N_2. The Y_{N_2} are practically straight lines of constant value and so the use of Eq. (9) to obtain flame speeds will not in general be reliable.

Figures A-1 and A-2 show the minor (H,OH,O and HO_2) and the major (H_2,O_2 H_2O and N_2) species profiles respectively. Figure A-3 shows the temperature and enthalpy profiles for transport method 6. Qualitatively there is little difference between these profiles and the corresponding ones of method 5, Figures 1,2, and 3 of the text. Figure A-4 shows three plots of the enthalpy, the function with the greatest observed difference. The solid line is the enthalpy computed using transport method 5, the dotted lines is method 6 and the dash-dot line is method 6 with the thermal diffusion set equal to zero. As can be seen almost all the difference between method 5 and method 6 can be attributed to the effects of thermal diffusion.

We add in passing that for transport method 6 with $D^T = 0$ the temperature and major species O_2, H_2O and N_2 practically overlaid the corresponding plots of both method 5 and method 6 ($D^T \neq 0$). For H_2 method 6 showed Y_{H_2} to decline at smaller values of x while methods 5 and 6 ($D^T = 0$) nearly overlapped.

The minor species profiles differences are characterized by the Y_i peak values as shown in Table A-2. At the peak and in the post-flame region the values for the minor species computed using method 6(D^T=0) were larger than the values computed using method 6($D^T \neq 0$) and these in turn were larger than the values computed using method 5.

The flame speed computed from the temperature profile for method 6($D^T = 0$) was 230 cms^{-1}. This is about 12% greater than the results of method 6($D^T \neq 0$). Warnatz's[22] computations are for a 45% H_2 in air premixed flame. In this case he finds that setting $D^T = 0$ raises the flame speed by $\sim$ 5%.

[22] *Warnatz, J. Ber. Bunsenges. Phys. Chem. 82, 643-649, (1978).*

TABLE A-1. COMPUTED FLAME SPEEDS METHOD VI

Variable	Flame[a] Velocity	Flame[b] Velocity
Temp.	208 cm/s	215 cm/s
H	207	221
OH	193	222
O	203	221
HO_2	-150	-3638
H_2	207	215
O_2	207	215
H_2O	207	215
N_2	205	154

a) $\psi_5 = 2.9$, $\epsilon = 3 \times 10^{-5}$, NINT = 24, NCN = 6, FC = 6.

b) Dixon-Lewis Kinetics[9]: $\psi_5 = 2.9$, $\epsilon = 3 \times 10^{-5}$, NINT = 24, NCN = 6, FC = 6.

TABLE A-2. COMPARISON OF RADICAL PEAK HEIGHTS AND ENTHALPY EXTREMA FOR TWO TRANSPORT ALGORITHMS.

Species	Function	Method 5	Method 6	Method 6(D^T=0)
H	$Y_{i(max)}$	2.6740E-3	2.6852E-3	2.8494E-3
	Temp.(K)	1353.8	1369.3	1364.6
	location(mm)	1.0935	1.1051	1.1049
OH	$Y_{i(max)}$	1.0012E-2	1.0356E-2	1.0409E-2
	Temp(K)	1968.6	1973.0	1965.8
	location(mm)	2.4838	2.4878	2.5436
O	$Y_{i(max)}$	7.5460E-3	7.8953E-3	7.9758E-3
	Temp.(K)	1408.9	1427.7	1499.1
	location(mm)	1.1399	1.1567	1.2452
HO_2	$Y_{i(max)}$	7.9263E-4	6.6590E-4	7.0769E-4
	Temp.(K)	369.0	382.2	377.2
	location(mm)	0.78185	0.76351	0.75791
enthalpy*	maximum	8.7725E+1	6.6526E+1	8.1928E+1
	Temp.(K)	916.9	901.8	928.5
	location(mm)	0.90429	0.89672	0.90314
enthalpy*	minimum	-2.2690E+1	-3.2441E+1	-2.3675E+1
	Temp.(K)	1479.5	1469.3	1484.7
	location(mm)	1.2143	1.2005	1.2269

* units of cal/gm

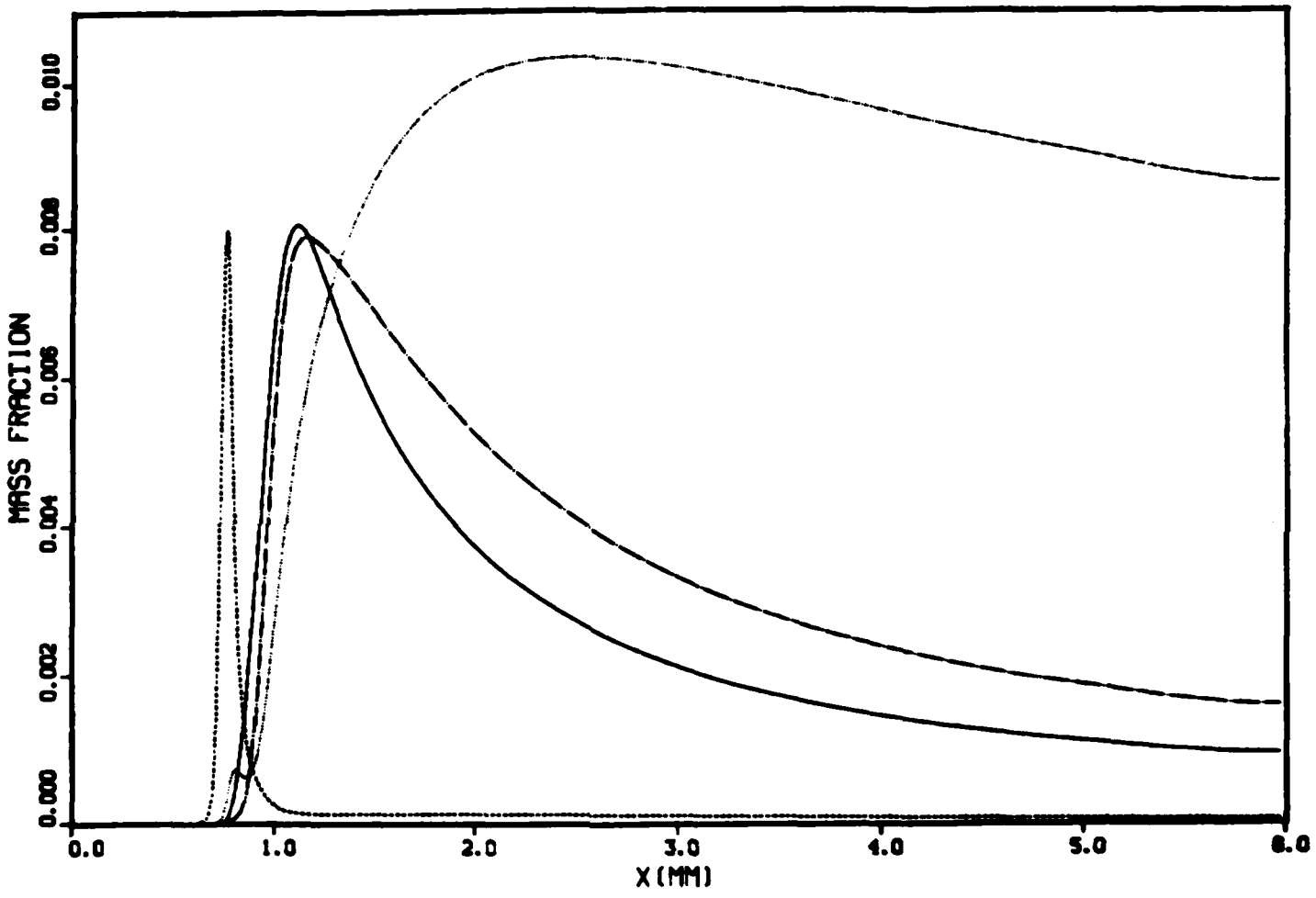

Fig. A-1. Radical species mass fraction profiles; H x 3 (—), OH (...), O (—.—.) and HO_2 x 12 (---). Transport method 6.

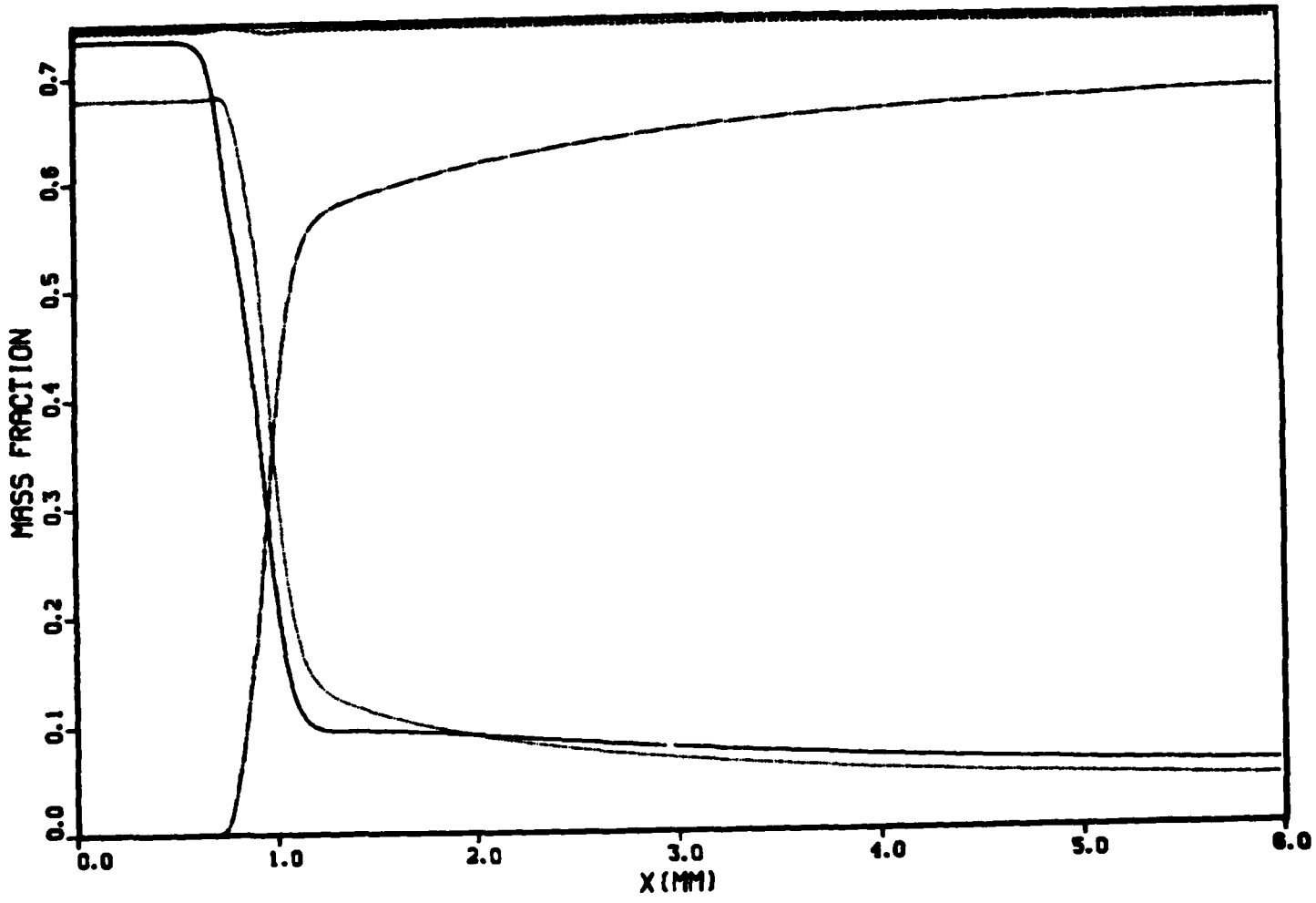

Fig. A-2. Major species mass fraction profiles; H_2 x 26 (—), O_2 x 3 (...), H_2O x 3 (—.—.) and N_2 (---). Transport method 6.

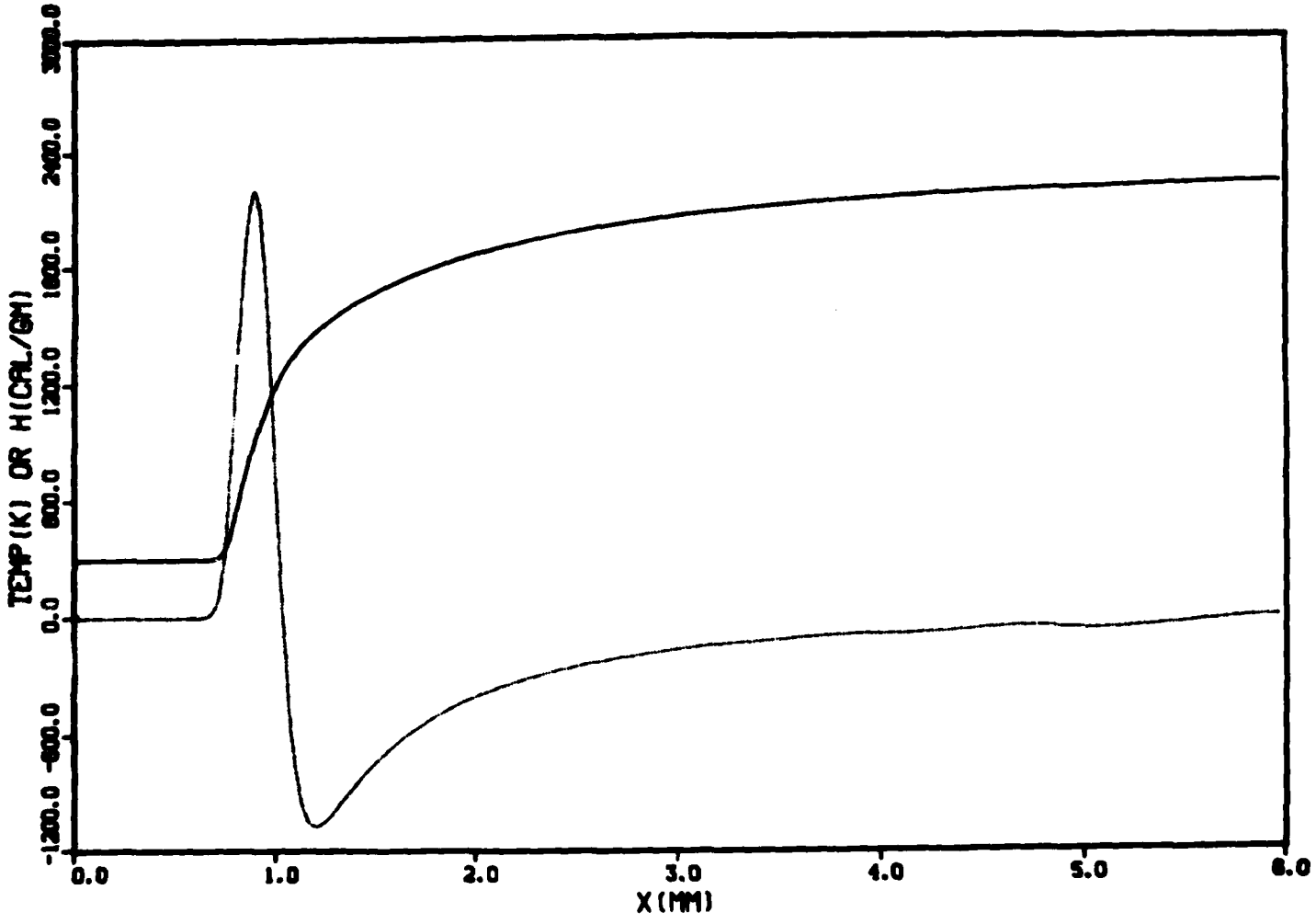

Fig. A-3. Temperature and enthalpy profiles. Temperature (—) and enthalpy x 33 (...). Transport method 6.

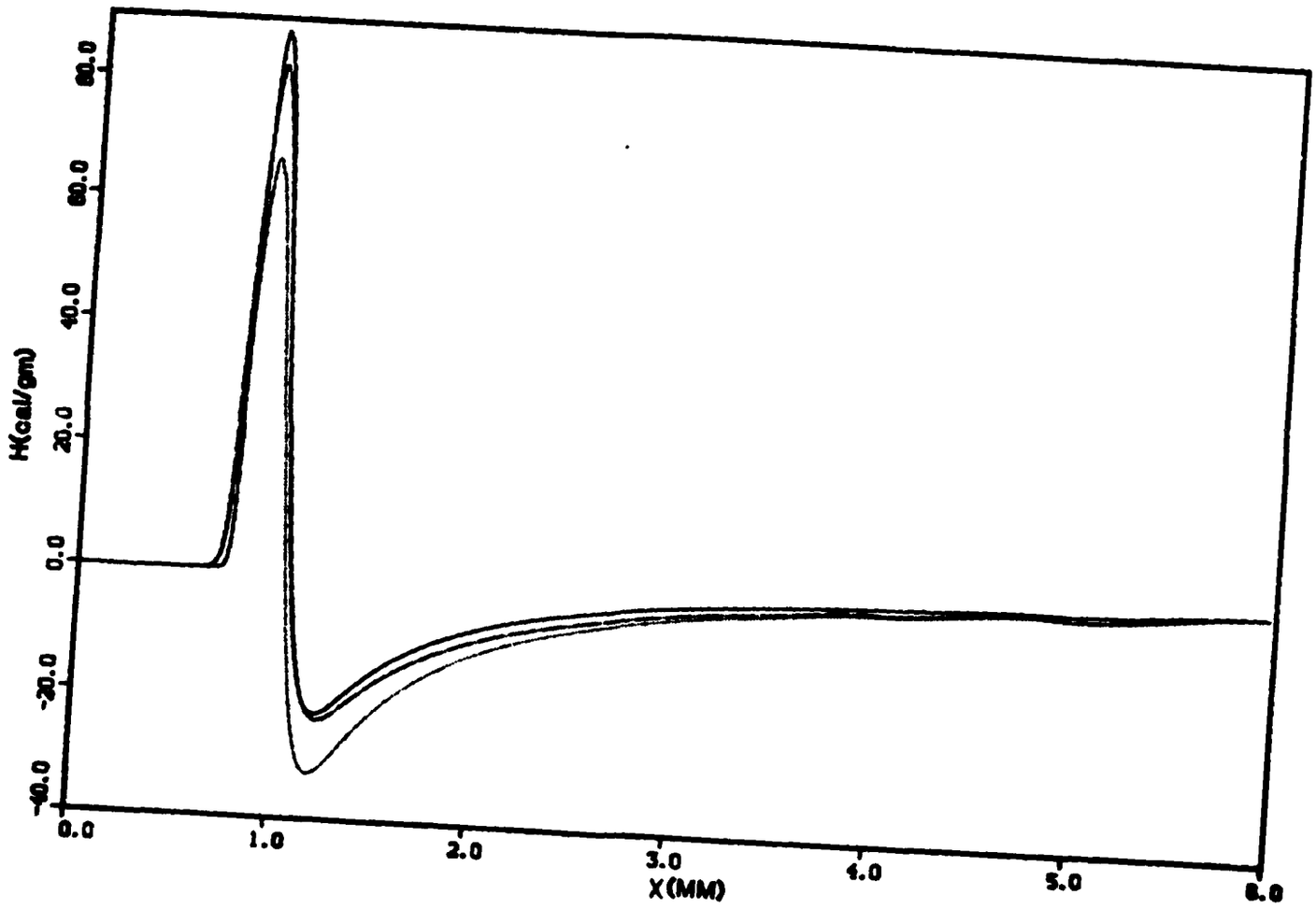

Fig. A-4. Enthalpy profiles; Method 5 (—), Method 6 (...), Method 6 with $D^T=0$ (—.—.).

GLOSSARY

C_p = heat capacity at constant pressure, cal-mole^{-1}-K^{-1}

c_p = $c_{pi}Y_i$, the specific heat of the mixture, cal-gm^{-1}-K^{-1}

c_{pi} = specific heat of ith species, cal-gm^{-1}-K^{-1}

D_{kj} = binary diffusion coefficients for species k and j, cm^2-s^{-1}

H_T^o = enthalpy, cal-mole^{-1}

h_i = specific enthalpy, cal-gm^{-1}

k = Boltzmann's constant, = 1.3806 erg - K^{-1}

k_i = rate coefficient for the ith reaction, in centimeter-mole-seconds units

N = number of species

M_i = molecular weight of ith species, gm-mole^{-1}

m_o = mass flux, gm-cm^{-2}-s^{-1}

P = total pressure, atmosphere

R = Gas constant, = 1.9872 cal-mole^{-1}K^{-1}, = 82.05 cm^3-atmos-mole^{-1}-K^{-1}

R_i = Rate of production of ith species by chemical reactions, mole-cm^{-3}-s^{-1}

S_u = burning velocity, cm-s^{-1}

T = temperature,K

T_B = temperature of burned mixture, K.

T_i^* = $T(\epsilon_i/K)^{-1}$

T_u = temperature of unburned mixture, K

t = temporal coordinate, s

u = fluid velocity, cm-s^{-1}

V_i = diffusion velocity of ith species, cm-s^{-1}

x = spatial coordinate, cm

x_i = mole fraction of ith species

Y_i = mass fraction of ith species

Y_{iB} = mass fraction of ith species in the burned mixture.

Y_{iu} = mass fraction of ith species in the unburned mixture.

ϵ_i/k= L-J or Stockmayer parameter, K

η_i = viscosity of ith species, gm-s^{-1}-cm^{-1}

λ = mixture conductivity, cal-cm^{-1}-s^{-1}-K^{-1}

λ_i = conductivity of ith species, cal-cm^{-1}-s^{-1}-K^{-1}

σ_i = L-J or Stockmayer parameter, 10^{-8}cm (= Å)

ρ = fluid density, gm-cm^{-3}

ψ = transformation coordinate (see equation 5), gm-cm^{-2}

$\Omega^{1,2}$,$\Omega^{2,2}$ = collision integrals (tabulated in reference 1)

DISTRIBUTION LIST

No. of Copies	Organization
12	Administrator Defense Technical Info Center ATTN: DTIC-DDA Cameron Station Alexandria, VA 22314
1	Director Defense Advanced Research Projects Agency ATTN: LTC. C. Buck 1400 Wilson Boulevard Arlington, VA 22209
2	Director Institute for Defense Analysis ATTN: H. Wolfhard R.T. Oliver 1801 Beauregard St. Alexandria, VA 22311
1	Commander US Army Materiel Development and Readiness Command ATTN: DRCDMD-ST 5001 Eisenhower Avenue Alexandria, VA 22333
4	Commander US Army Armament Research and Development Command ATTN: DRDAR-LCA, J. Lannon DRDAR-LC, T. Vladimiroff DRDAR-LCE, R.F. Walker DRDAR-SCA, L. Stiefel Dover, NJ 07801
2	Commander US Army Armament Research & Development Command ATTN: DRDAR-TSS Dover, NJ 07801
1	Commander US Army Armament Research & Development Command ATTN: DRDAR-TDC Dover, NJ 07801
1	Commander US Army Armament Materiel Readiness Command ATTN: DRSAR-LEP-L, Tech Lib Rock Island, IL 61299
1	Commander US Army Watervliet Arsenal ATTN: Code SARWV-RD, R. Thierry Watervliet, NY 12189
1	Director US Army ARRADCOM Benet Weapons Laboratory ATTN: DRDAR-LCB-TL Watervliet, NY 12189
1	Commander US Army Aviation Research and Development Command ATTN: DRDAV-E 4300 Goodfellow Blvd St. Louis, MO 63120
1	Director US Army Air Mobility Research and Development Laboratory Ames Research Center Moffett Field, CA 94035
1	Commander US Army Communications Rsch and Development Command ATTN: DRDCO-PPA-SA Ft. Monmouth, NJ 07703
1	Commander US Army Electronics Research & Development Command Technical Support Activity ATTN: DELSD-L Fort Monmouth, NJ 07703
2	Commander US Army Missile Command ATTN: DRSMI-R DRSMI-YDL Redstone Arsenal, AL 35898

DISTRIBUTION LIST

No. of Copies	Organization
1	Commander US Army Natick Research and Development Command ATTN: DRXRE, D. Sieling Natick, MA 01762
1	Commander US Army Tank Automotive Rsch and Development Command ATTN: DRDTA-UL Warren, MI 48090
1	Commander US Army White Sands Missile Range ATTN: STEWS-DP-AL WSMR, NM 88002
1	Commander US Army Materials & Mechanics Research Center ATTN: DRXMR-ATL Watertown, MA 02172
5	Commander US Army Research Office ATTN: Tech Lib D. Squire F. Schmiedeshaff R. Ghirardelli M. Ciftan P. O. Box 12211 Research Triangle Park, NC 27706
1	Director US Army TRADOC Systems Analysis Activity ATTN: ATAA-SL, Tech Lib White Sands Missile Range NM 88002
1	Commander Naval Research Laboratory ATTN: Dr. E. Oran, Code 4040 Washington, DC 20375
1	Office of Naval Research Dept of the Navy ATTN: Code 473 G. Neece 800 N. Quincy Street Arlington, VA 22217
1	Commander Naval Sea Systems Command ATTN: J.W. Murrin (NAVSEA-62R2) National Center Building 2, Room 6E08 Washington, DC 20362
2	Commander Naval Surface Weapons Center ATTN: S.J. Jacobs/Code 240 Code 730 Silver Springs, MD 20910
1	Commander Naval Surface Weapons Center ATTN: Library Br, DX-21 Dahlgren, VA 22448
1	Commander Naval Underwater Systems Center Energy Conversion Department ATTN: R.S. Lasar/Code 5B331 Newport, RI 02840
2	Commander Naval Weapons Center ATTN: R. Derr C. Thelen China Lake, CA 93555
1	Commander Naval Research Laboratory ATTN: Code 6180 Washington, DC 20375
3	Superintendent Naval Post Graduate School ATTN: Tech Lib D. Netzer A. Fuhs Monterey, CA 93940

DISTRIBUTION LIST

No. of Copies	Organization
2	Commander Naval Ordnance Station ATTN: S. Mitchell Tech Lib Indian Head, MD 20640
2	AFOSR ATTN: L. Caveny B.T. Wolfson Bolling AFB, DC 20332
2	AFRPL (DYSC) ATTN: D. George J.N. Levine Edwards AFB, CA 93523
2	National Bureau of Standards ATTN: J. Hastie T. Kashiwagi Washington, DC 20234
1	Lockheed Missile & Space Co. ATTN: Tech Info Ctr 3521 Hanover Street Palo Alto, CA 94304
1	Aerojet Solid Propulsion Co. ATTN: P. Micheli Sacramento, CA 95813
1	ARO Incorporated ATTN: D. Dougherty Arnold AFB, TN 37389
1	Atlantic Research Corporation ATTN: M.K. King 5390 Cherokee Avenue Alexandria, VA 22314
1	AVCO Everett Research Lab ATTN: D. Stickler 2385 Revere Beach Parkway Everett, MA 02149
2	Calspan Corporation ATTN: E.B. Fisher A.P. Trippe P.O. Box 400 Buffalo, NY 14225
1	Olin Corporation Badger Army Ammunition Plant ATTN: J. Ramnarace Baraboo, WI 53913
1	Foster Miller Associates ATTN: A.J. Erickson 135 Second Avenue Waltham, MA 02154
1	General Electric Company Armament Department ATTN: M.J. Bulman Lakeside Avenue Burlington, VT 05402
1	General Electric Company Flight Propulsion Division ATTN: Tech Lib Cincinnati, OH 45215
1	General Motors Research Laboratories Physics Department ATTN: C. Dasch Warren, MI 48090
2	Hercules Powder Co. Allegheny Ballistics Lab. ATTN: R. Miller Tech Lib Cumberland, MD 21501
1	Hercules Incorporated Bacchus Works ATTN: B. Isom Magna, UT 84044

DISTRIBUTION LIST

No. of Copies	Organization
1	Paul Gough Associates, Inc. ATTN: P. S. Gough P. O. Box 1614 Portsmouth, NH 03801
1	Physics International Company 2700 Merced Street Leandro, CA 94577
1	Pulsepower Systems, Inc. ATTN: L. C. Elmore 815 American Street San Carlos, CA 94070
3	Rockwell International Corp. Rocketdyne Division ATTN: C. Obert J. E. Flanagan A. Axeworthy 6633 Canoga Avenue Canoga Park, CA 91304
1	Hercules, Inc. Industrial Systems Dept P. O. Box 548 ATTN: W. Haymes Tech Lib McGregor, TX 76657
1	SAI ATTN: R. Farmer 21133 Victory Boulevard Suite 216 Canoga Park, CA 91303
1	Science Applications, Inc. ATTN: R. B. Edelman Combustion Dynamics & Propulsion Division 23146 Cumorah Crest Woodland Hills, CA 91364
1	Shock Hydrodynamics, Inc. ATTN: W. H. Anderson 4710-16 Vineland Avenue North Hollywood, CA 91602
1	Thiokol Corporation Elkton Division ATTN: E. Sutton Elkton, MD 21921
3	Thiokol Corporation Huntsville Division ATTN: D. Flanigan R. Glick Tech Lib Huntsville, AL 35807
2	Thiokol Corporation Wasatch Division ATTN: J. Peterson Tech Lib P. O. Box 524 Brigham City, UT 84302
1	TRW Systems Group ATTN: H. Korman One Space Park Redondo Beach, CA 90278
2	United Technologies Chemical Systems Division ATTN: R. Brown Tech Lib Sunnyvale, CA 94086
1	Universal Propulsion Co. ATTN: H. J. McSpadden Black Canyon Stage 1, Box 1140 Phoenix, AZ 85029

DISTRIBUTION LIST

No. of Copies	Organization
1	IITRI ATTN: M. J. Klein 10 West 35th Street Chicago, IL 60616
1	Battelle Memorial Institute ATTN: Tech 505 King Avenue Columbus, OH 43201
1	Brigham Young University Dept of Chemical Engineering ATTN: M. W. Beckstead Provo, UT 84601
1	California Institute of Tech 204 Kamar Lab Mail Stop 301-46 ATTN: F. E. C. Culick 1201 E. California Street Pasadena, CA 91125
1	Case Western Reserve Univ. Division of Aerospace Sciences ATTN: J. Tien Cleveland, OH 44135
3	Georgia Institute of Technology School of Aerospace Engineering ATTN: B. T. Zinn E. Price W. C. Strahle Atlanta, GA 30332
1	Institute of Gas Technology ATTN: D. Gidaspow 3424 S. State Street Chicago, IL 60616
1	Johns Hopkins University/APL Chemical Propulsion Information Agency ATTN: T. Christian Johns Hopkins Road Laurel, MD 20707
1	Massachusetts Institute of Technology Dept of Mechanical Engineering ATTN: T. Toong Cambridge, MA 02139
1	Princeton Combustion Rsch Center ATTN: M. Summerfield 1041 US Highway One North Princeton, NJ 08540
1	Pennsylvania State University Applied Research Lab ATTN: G. M. Faeth P. O. Box 30 State College, PA 16801
1	Pennsylvania State University Dept of Mechanical Engineering ATTN: K. Kuo University Park, PA 16802
1	Pennsylvania State University Dept of Material Sciences ATTN: H. Palmer University Park, PA 16802
1	Princeton University Forrestal Campus ATTN: I. Glassman Tech Lib P. O. Box 710 Princeton, NJ 08540

DISTRIBUTION LIST

No. of Copies	Organization
2	Purdue University School of Mechanical Engineering ATTN: J. Osborn S. N. B. Murphy TSPC Chaffee Hall West Lafayette, IN 47906
1	Rutgers State University Dept of Mechanical and Aerospace Engineering ATTN: S. Temkin University Heights Campus New Brunswick, NJ 08903
1	Southwest Research Institute Fire Research Section ATTN: W. H. McLain 8500 Culebra Road San Antonio, TX 78228
4	SRI International ATTN: Tech Lib J. Barker D. Corsley D. Golden 333 Ravenswood Avenue Menlo Park, CA 94025
1	Stevens Institute of Technology Davidson Laboratory ATTN: R. McAlevy, III Hoboken, NJ 07030
1	University of California, San Diego Ames Department ATTN: F. Williams P. O. Box 109 La Jolla, CA 92037
1	University of Illinois Dept. of Mechanical Engineering 144 MEB, 1206 W. Green St. Urbana, IL 61801
1	University of Minnesota Dept of Mechanical Engineering ATTN: E. Fletcher Minneapolis, MN 55455
1	University of Southern California Dept of Chemistry ATTN: S. Benson Los Angeles, CA 90007
2	University of Texas Dept of Chemistry ATTN: W. Gardiner H. Schaefer Austin, TX 78712
1	Rensselaer Polytechnic Institute ATTN: Prof. A. Fontijn Troy, N. Y. 12181
3	Center for Non Linear Studies ATTN: Dr. Basil Nichols Mail Stop 457 Los Alamos National Laboratory Los Alamos, New Mexico 87545
1	Princeton University Department of Mechanical and Aerospace Engineering ATTN: Prof. Rolf D. Reitz Princeton, NJ 08540
2	University of Utah Dept of Chemical Engineering ATTN: A. Baer G. Flandro Salt Lake City, UT 84112

DISTRIBUTION LIST

Aberdeen Proving Ground

Dir, USAMSAA
ATTN: DRXSY-D
DRXSY-MP, H. Cohen

Cdr, USATECOM
ATTN: DRSTE-TO-F

Dir, USCSL, Bldg. E3516, EA
ATTN: DRDAR-CLB-PA


DATE
FILME
0-8